# Discrimination between wave-ravinement surfaces and bedset boundaries in Pliocene shallow-marine deposits, Crotone Basin, southern Italy: An integrated sedimentological, micropalaeontological and mineralogical approach

MASSIMO ZECCHIN*, MAURO CAFFAU*, OCTAVIAN CATUNEANU† and DAVIDE LENAZ‡
*Istituto Nazionale di Oceanografia e di Geofisica Sperimentale - OGS, 34010 Sgonico (TS), Italy (E-mail: mzecchin@ogs.trieste.it)
†Department of Earth and Atmospheric Sciences, University of Alberta, 1-26 Earth Sciences Building, Edmonton, Alberta T6G 2E3, Canada
‡Dipartimento di Matematica e Geoscienze, Università di Trieste, 34127 Trieste, Italy

**ABSTRACT**

The lower Pliocene Belvedere Formation, cropping out in the Crotone Basin, southern Italy, exhibits a metre-scale to decametre-scale shallow-marine cyclicity that shares features of both high-frequency sequences linked to shoreline shifts and controlled by minor relative sea-level and/or sediment supply changes, and sedimentological cycles unrelated to shoreline shifts. In order to better understand the high-frequency sequence stratigraphic framework of this succession, an integration of sedimentological, micropalaeontological (micro-foraminifera assemblages) and mineralogical (heavy mineral abundance) data is used. From a sedimentological/stratigraphic point of view, wave-ravinement surfaces bounding high-frequency sequences, and associated substrate-controlled ichnofacies, are prominent in outcrop and document environmental and water-depth changes, whereas bedset boundaries separating sedimentological cycles have a more subtle field appearance and are only associated with changes of environmental energy. Moreover, condensed deposits are present only above wave-ravinement surfaces, and the high-frequency sequences bounded by these surfaces have a thickness that is an order of magnitude greater than that of the bedsets. Micro-foraminifera assemblages may change, and the content of heavy minerals usually increases, across wave-ravinement surfaces, whereas both parameters do not change significantly across bedset boundaries. The abundance of heavy minerals is systematically higher, with respect to the underlying and overlying deposits, in the condensed shell beds that overlie wave-ravinement surfaces. An integrated sedimentological, micropalaeontological and mineralogical approach represents a powerful tool to discriminate between wave-ravinement surfaces bounding high-frequency sequences and bedset boundaries, and in general to investigate at the intra high-frequency sequence scale. This integrated approach is expected to be very useful in the study of potentially all shallow-marine successions composed of small-scale cycles, in order to delineate a detailed sequence stratigraphic framework and understand the factors that controlled the cyclicity.

**Keywords** Bedset, facies analysis, heavy minerals, high-frequency sequence, micropalaeontology, wave-ravinement surface.

## INTRODUCTION

Wave-ravinement surfaces (WRSs) are erosional, diachronous surfaces having sequence stratigraphic significance, which are produced by waves in the shoreface during transgression; they are often mantled by transgressive lags and/or shell concentrations and may be marked by substrate-controlled ichnofossils (Cattaneo & Steel, 2003; Catuneanu, 2003, 2006; Demarest & Kraft, 1987; Hwang & Heller, 2002; Kidwell, 1991; Naish & Kamp, 1997a; Nummedal & Swift, 1987; Pemberton *et al.*, 1992; Posamentier & Allen, 1999; Swift, 1968; Zecchin & Catuneanu, 2013). Wave-ravinement surfaces usually have a very good physical appearance in both outcrops and cores, as well as in high-resolution seismic data, because they separate shallow-marine deposits (above) from continental and/or back-barrier deposits (below) and may rework older sequence stratigraphic surfaces becoming systems tract and/or sequence boundaries (e.g. Catuneanu, 2003, 2006; Demarest & Kraft, 1987; Mellere *et al.*, 2005; Nummedal & Swift, 1987; Steel *et al.*, 2000; Swift, 1968; Zecchin & Catuneanu, 2013; Zecchin *et al.*, 2009).

At the scale of the fourth-order or lower rank cycles, corresponding to high-frequency sequences (Catuneanu & Zecchin, 2013; Zecchin & Catuneanu, 2013) or parasequences (Van Wagoner *et al.*, 1988, 1990), and in the case of low-magnitude relative sea-level changes and/or minor sediment supply variations, WRSs and transgressive surfaces in general are associated with limited landward facies shift and shoreline transgression. In such cases, WRSs may be found within fully shoreface deposits and may be difficult to distinguish from surfaces bounding sedimentological cycles unrelated to shoreline shifts, such as bedsets (Van Wagoner *et al.*, 1990) (Fig. 1A and B). Bedsets are sedimentary units that record local variations in sediment supply, climate and autocyclic processes (Hampson *et al.*, 2008; Sømme *et al.*, 2008), with their boundaries corresponding to either non-depositional or erosional discontinuities (Fig. 1B); they are usually well recognizable in lower shoreface and inner shelf settings (Hampson, 2000; Sømme *et al.*, 2008).

To avoid confusion with high-frequency sequences, Zecchin & Catuneanu (2013)

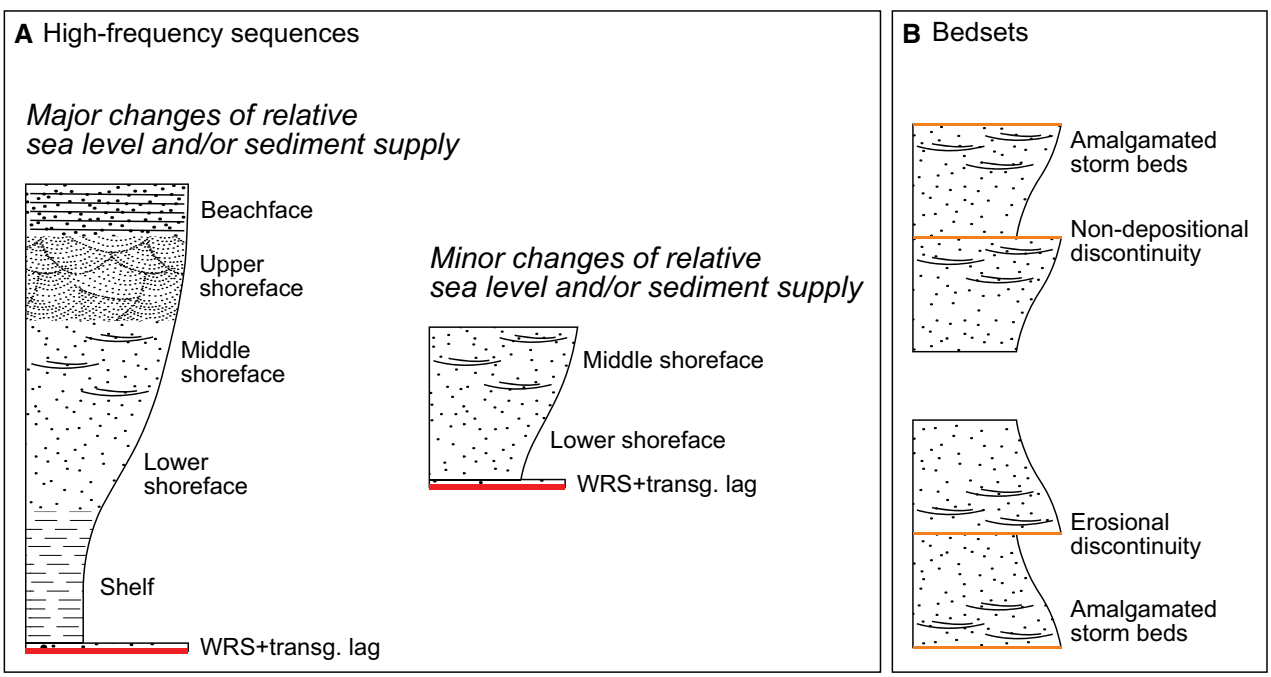


**Fig. 1.** (A) Comparison between high-frequency sequences showing a parasequence-like architecture but controlled by relative sea-level and/or sediment supply changes of different magnitude. (B) Typical architectures of bedsets bounded by non-depositional discontinuities (above) and erosional discontinuities (below), and controlled by autocyclic processes unrelated to shoreline shifts (see text). Note the similarity between bedsets and high-frequency sequences controlled by minor changes of relative sea-level and/or sediment supply. WRS, wave-ravinement surface.

recommended the use of bedsets for small (metre-scale) cycles that form independently of transgressions and regressions and that are recognizable only for relatively short distances along depositional dip and strike. However, bedset boundaries may be confused with flooding surfaces and high-frequency WRSs or regressive surfaces of marine erosion (RSME; Plint, 1988; Plint & Nummedal, 2000) linked to metre-scale relative sea-level changes (Fig. 1A and B), especially where shoreline shifts cannot be observed directly in the field (e.g. Hampson *et al.*, 2011). New tools are therefore necessary to discriminate between small-scale cycles related to shoreline shifts (i.e. high-frequency sequences) and sedimentological cycles. The ability to recognize sequences in fully shallow-marine deposits is essential to achieve a detailed sequence stratigraphic framework and to fully understand the controls on sediment supply and accommodation development for a given succession.

In order to discriminate between surfaces of sequence stratigraphic significance and bedset boundaries, and ultimately between high-frequency sequences and bedsets, the case study of the lower Pliocene shallow-marine Belvedere Formation, cropping out in the Crotone Basin, southern Italy, is shown (Figs 2 to 4). Previous studies have highlighted that this normal fault-bounded, highly aggradational succession is composed of metre-scale cycles inferred to record minor relative sea-level changes and climate variations (Zecchin, 2005) (Fig. 5). The boundaries of such cycles as well as of smaller units, having features that resemble those of both high-frequency WRSs and erosional discontinuities bounding bedsets, are documented in detail in this study.

The aim of this study was the development of a new tool, based on an integrated sedimentological, micropalaeontological and mineralogical approach, to discriminate between high-frequency WRSs and bedset boundaries. In particular, traditional facies analysis is combined with the analysis of benthic foraminifera associations as well as with a measurement of the abundance of heavy minerals in the studied deposits. The concentration of heavy minerals on the siliciclastic shelf sediments tends to increase landward, reaching a maximum in the beachface due to selective winnowing (Komar, 2007; Roy, 1999). However, wave reworking and offshore bypass of finer and lighter sediment particles associated with the formation of WRSs are expected to lead to an enrichment of heavy minerals in the condensed deposits that overlie such surfaces, with respect to the underlying and overlying sediments. Transgressive lags are already known to contain placer deposits (Catuneanu & Biddulph, 2001); however, the use of heavy mineral concentrations in sequence stratigraphic analysis was surprisingly neglected in the past, despite the fact that this criterion may potentially be useful to recognize surfaces of sequence stratigraphic significance. This is particularly true if several independent criteria, in addition to mineralogical, are combined, as presented in this study. Such an integrated approach may be useful in all cases where the outcrop extent is limited or cores are sparse, and represents a valuable tool in all studies dealing with high-resolution sequence stratigraphy and with investigations at the intra high-frequency sequence scale.

## GEOLOGICAL SETTING

### The Calabrian Arc and the Crotone Basin

The Calabrian Arc is an arcuate terrane located between the north-west-trending southern Apennines and the east-trending Sicilian Maghrebides, and separates the Ionian and Tyrrhenian basins (Fig. 2A). It consists of both metamorphic and sedimentary units, including Hercynian and pre-Hercynian continental basement and Jurassic to Early Cretaceous ophiolite-bearing sequences (Amodio Morelli *et al.*, 1976; Bonardi *et al.*, 2001). The Calabrian Arc migrated south-eastward from mid-Miocene onward in response to the subduction of the Ionian oceanic lithosphere along a deep and narrow Benioff zone (Bonardi *et al.*, 2001; Faccenna *et al.*, 2001, 2004; Malinverno & Ryan, 1986; Sartori, 2003). The movement towards the south-east caused a fragmentation of the arc in individual blocks bounded by north-west-trending shear zones, which controlled the development of basins located along both the Ionian and Tyrrhenian sides of Calabria (Knott & Turco, 1991) (Fig. 2A). Since the middle Pleistocene, the Calabrian Arc experienced rapid uplift of up to *ca* 1 mm year$^{-1}$ (Westaway, 1993) that persists today, as documented by flights of marine terraces developed along the coasts.

Along the Ionian side of the Calabrian Arc, the Ionian forearc Basin developed internally with respect to the accretionary wedge since the late Oligocene (Bonardi *et al.*, 2001; Cavazza &

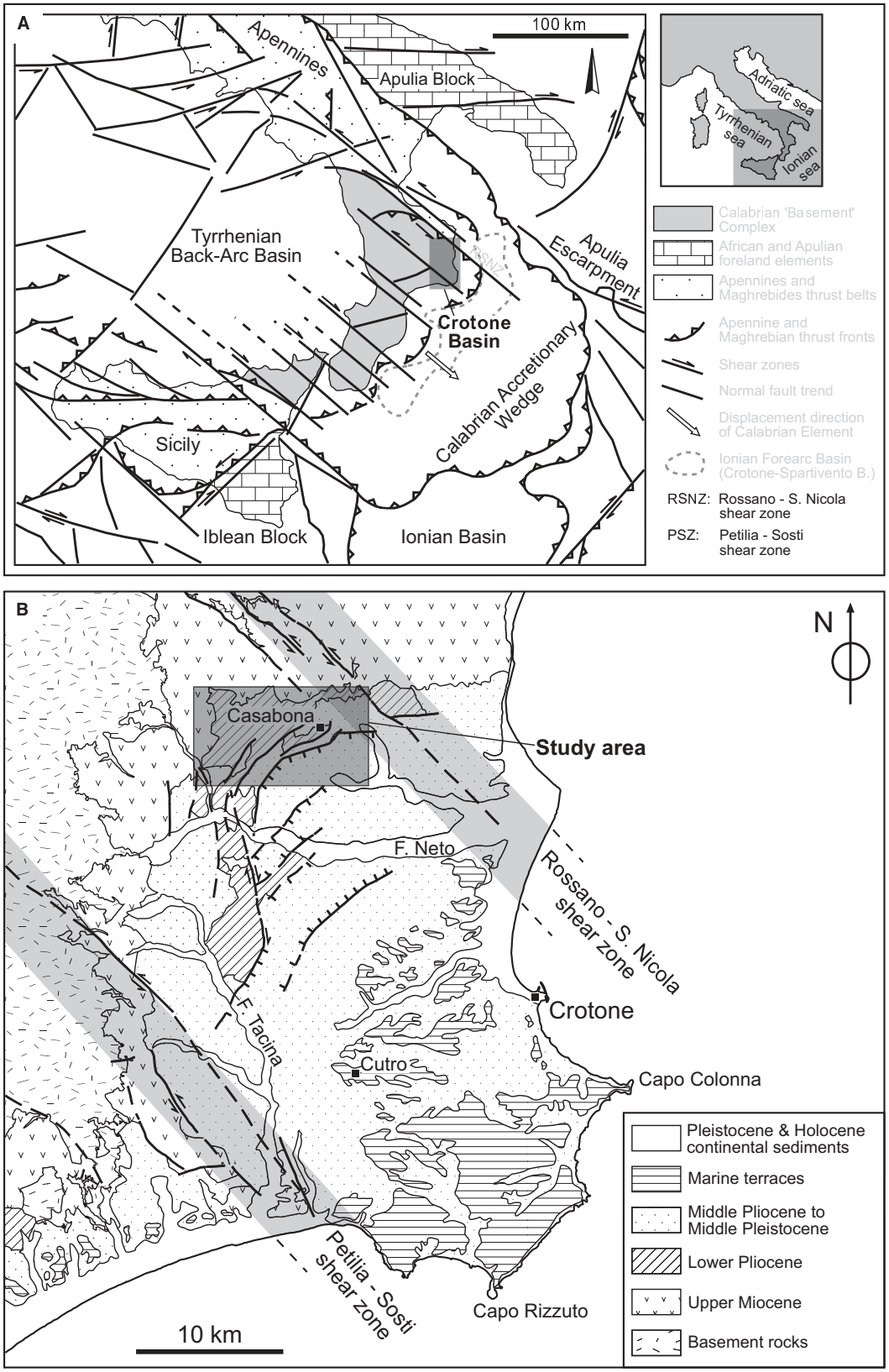


**Fig. 2.** (A) Structural map of the Calabrian Arc and location of the Crotone Basin (modified from Van Dijk & Okkes, 1991). Note the north-west trending shear zones that dissect the Calabrian complex. (B) Simplified geological map of the Crotone Basin showing the study area (modified from Zecchin *et al.*, 2004).

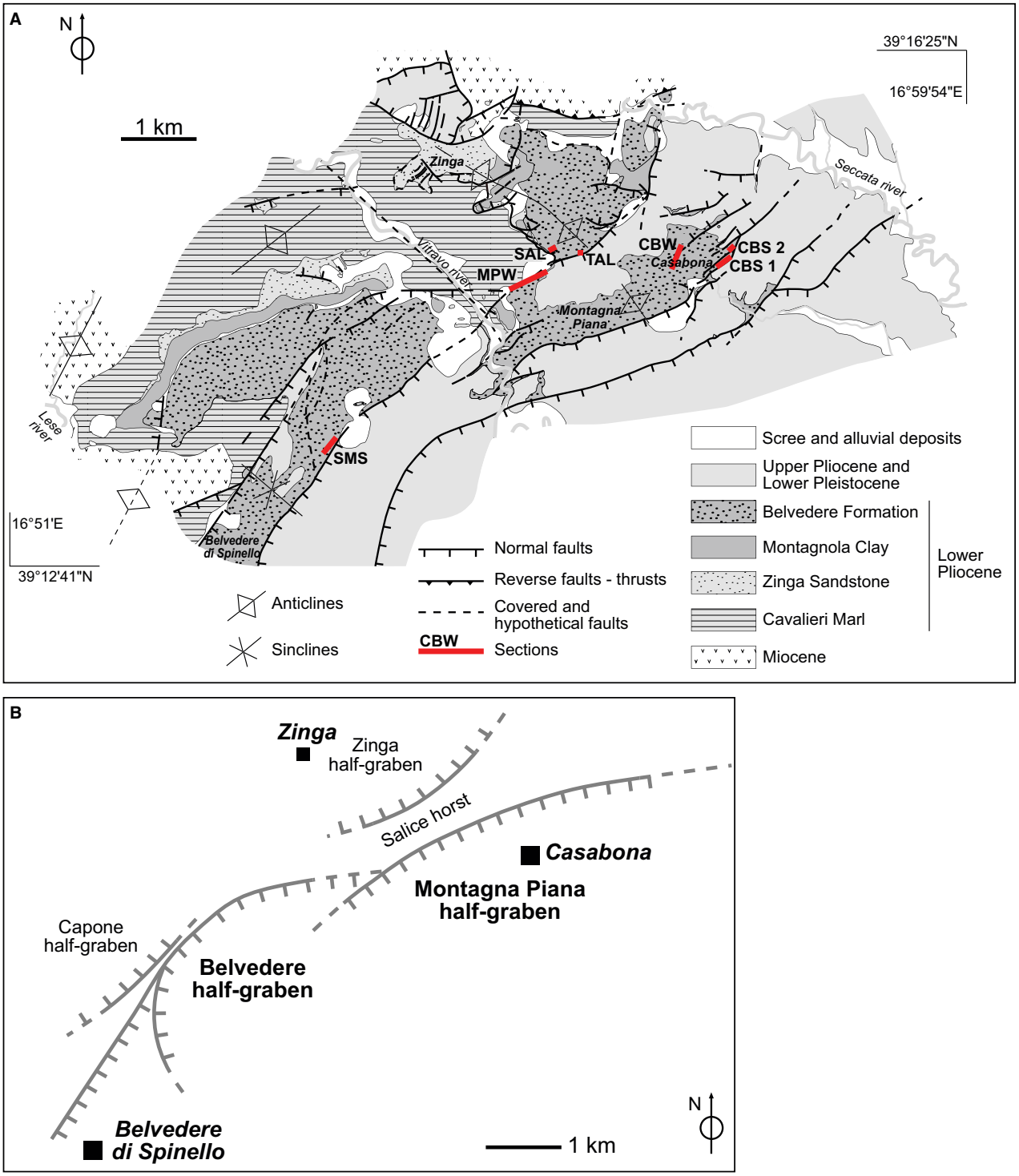


**Fig. 3.** (A) Geological map of the north-western part of the study area in the Crotone Basin, showing the location of measured sections (modified from Zecchin, 2005 and Zecchin & Caffau, 2012). CBS 1, South Casabona 1 section; CBS 2, South Casabona 2 section; CBW, West Casabona section; MPW, West Montagna Piana section; SAL, Salice section; SMS, Santa Maria della Scala section; TAL, Tallarico section. (B) Half-graben sub-basins active during deposition of the Belvedere Formation in the northern part of the Crotone Basin (modified from Zecchin *et al.*, 2004).

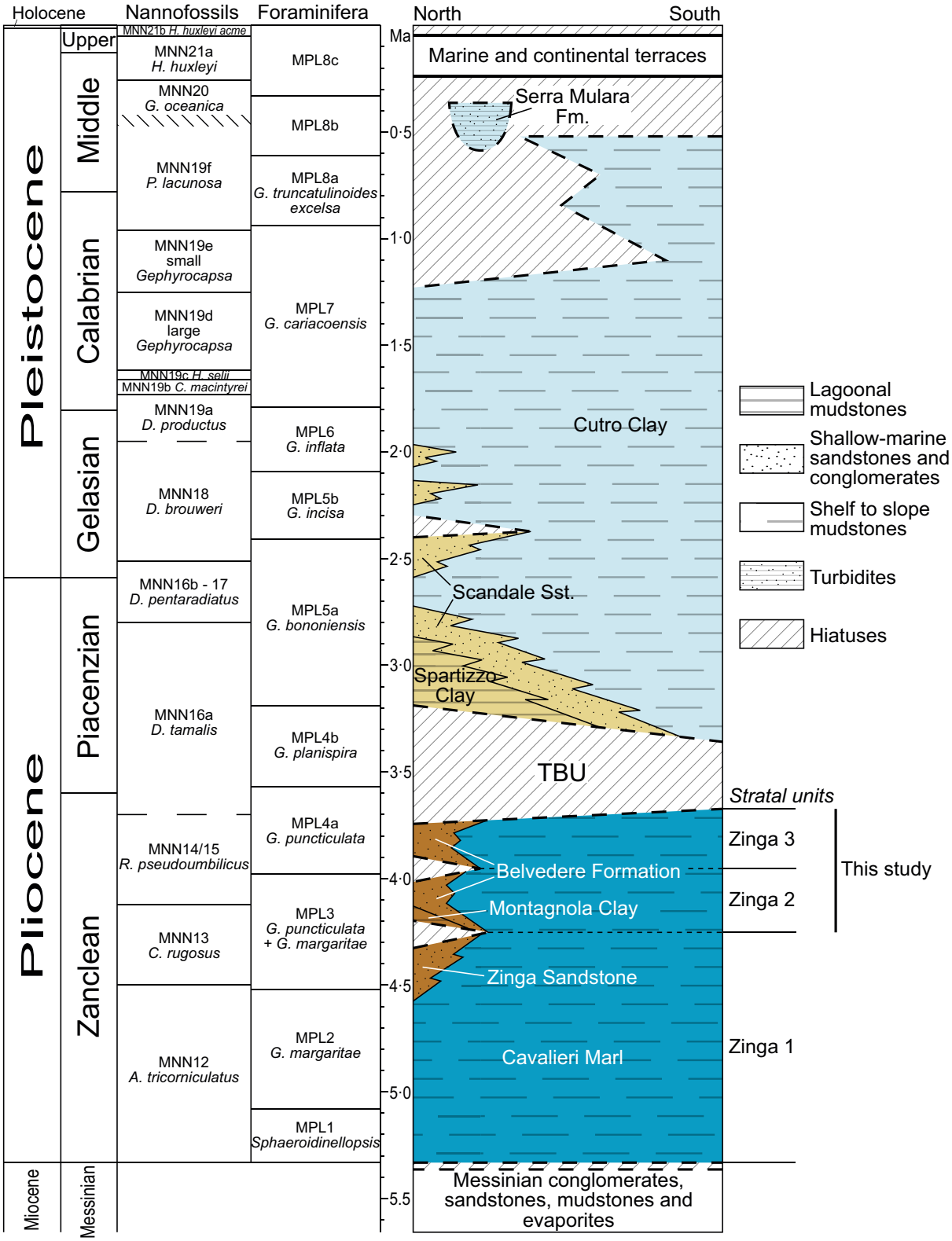


**Fig. 4.** The Plio-Pleistocene succession of the Crotone Basin (modified from Zecchin *et al.*, 2012, 2015, 2016). This study is focused on the lower Pliocene Belvedere Formation, cropping out in the northern part of the basin. The chronostratigraphic scheme is from Gibbard *et al.* (2010), and the calcareous nannofossil and planktonic foraminifera biostratigraphic schemes and their chronology are from Cita (1975), Rio *et al.* (1990), Lourens *et al.* (1996) and Raffi *et al.* (2006). TBU, Timpa Biso Unconformity.

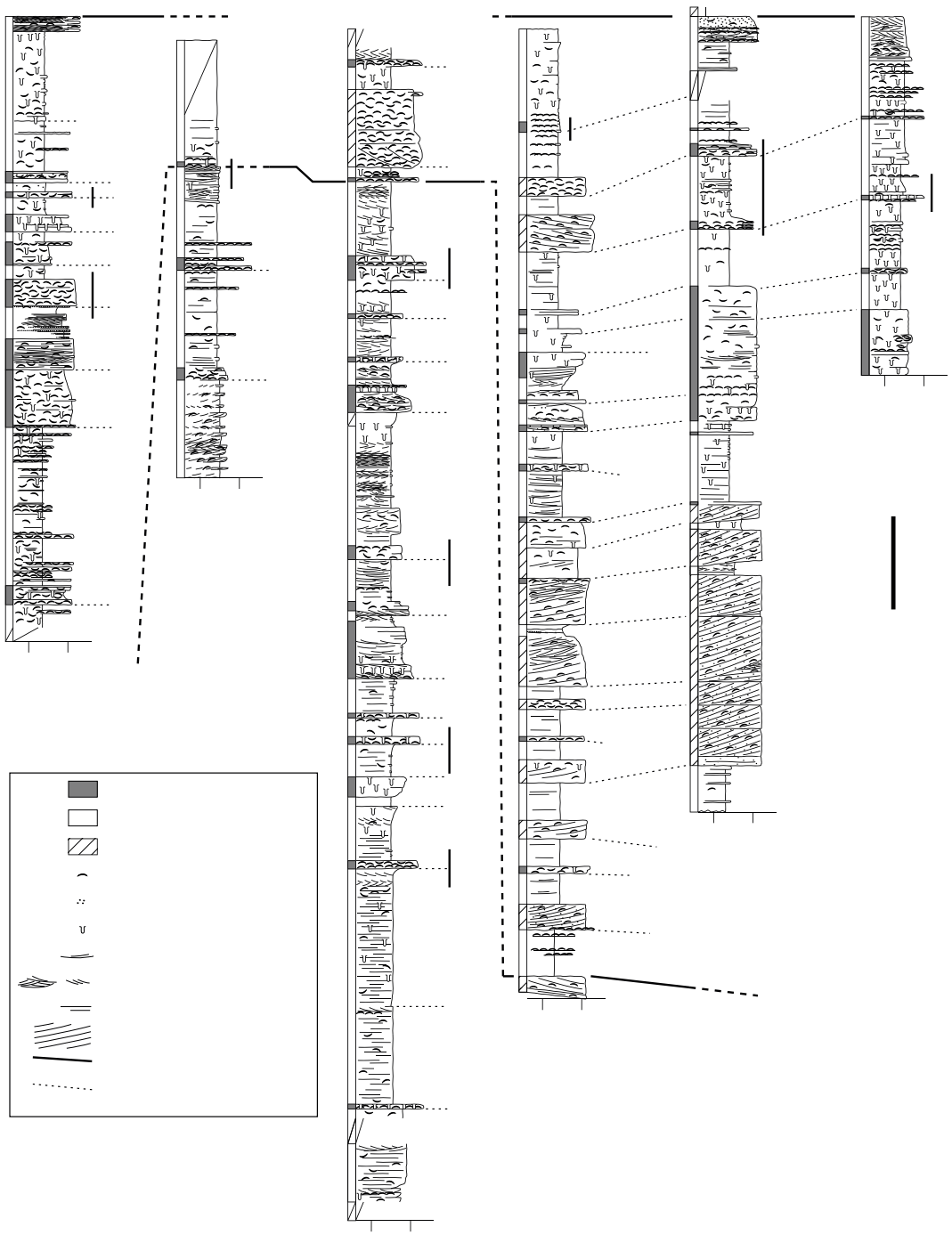

**Fig. 5.** The measured sections considered in this study, documenting part of the lower Pliocene Belvedere Formation (see Fig. 3A for locations; modified from Zecchin, 2005). The studied succession accumulated in the Montagna Piana and Belvedere half-graben sub-basins, and on the Salice horst (see Fig. 3B). The details of the sections shown in Figs 7 to 10 are indicated. Note that the Tallarico (TAL, Fig. 3A) section is not illustrated here. Facies associations A and B are summarized in Table 1 and described in the text. CBS 1, South Casabona 1 section; CBS 2, South Casabona 2 section; CBW, West Casabona section; MPW, West Montagna Piana section; SAL, Salice section; SMS, Santa Maria della Scala section; TBU, Timpa Biso Unconformity; Zn 2 – Zinga 2 stratal unit; Zn 3 – Zinga 3 stratal unit; cs = cross-stratification.

Barone, 2010; Cavazza & DeCelles, 1993) (Fig. 2A). It is composed of parts currently uplifted and cropping out along the Ionian coast, such as the Crotone Basin, and of a main active area known to as the Crotone–Spartivento Basin (Fig. 2A).

The Crotone Basin is bounded to the north and to the south by two north-west-trending left-lateral shear zones, called Rossano-San Nicola and Petilia-Sosti, respectively (Meulenkamp *et al.*, 1986; Van Dijk, 1990, 1991, 1994; Van Dijk & Okkes, 1991) (Fig. 2A and B). It began to open between Serravallian and Tortonian times (Roda, 1964; Van Dijk, 1990) and contains a sedimentary succession consisting of upper Serravallian to middle Pleistocene continental, back-barrier, shallow-marine, shelf and slope deposits organized into tectono-stratigraphic units of different hierarchy (Massari & Prosser, 2013; Roda, 1964; Van Dijk, 1990; Zecchin *et al.*, 2004, 2012) (Fig. 4). The tectonic history of the Crotone Basin was characterized by a dominant extensional tectonic regime that was interrupted periodically by relatively short compressional and transpressional phases in mid-Messinian, mid-Pliocene and earliest and mid-Pleistocene times, which involved the whole Calabrian Arc (Massari & Prosser, 2013; Van Dijk, 1990, 1991; Zecchin *et al.*, 2012, 2015). Since the latest middle Pleistocene, uplift has led to the emergence of the basin (Cosentino *et al.*, 1989; Zecchin *et al.*, 2012, 2016).

## The lower Pliocene succession of the Crotone Basin

The lower Pliocene succession is well-exposed in the north-western part of the Crotone Basin, where it consists of the Cavalieri Marl (shelf to slope), the Zinga Sandstone (shoreface to deltaic), the Montagnola Clay (lagoonal) and the Belvedere Formation (shallow-marine) (Zecchin *et al.*, 2003, 2004, 2006, 2012) (Figs 3A and 4). Near the basin margin, these formations compose three unconformity bounded stratal units, which correspond to depositional sequences bounded by subaerial unconformities or maximum regressive surfaces locally reworked by ravinement surfaces: Zinga 1 (Cavalieri Marl and Zinga Sandstone), Zinga 2 (top of the Zinga Sandstone, Montagnola Clay and lower part of the Belvedere Formation) and Zinga 3 (upper part of the Belvedere Formation) (Zecchin *et al.*, 2003, 2004, 2006, 2012) (Fig. 4). The lower Pliocene succession is capped by the Timpa Biso Unconformity (TBU; Figs 4 and 5), which is a subaerial unconformity associated with a main tectonic event (see Consolaro *et al.*, 2013 and Zecchin *et al.*, 2012, and references therein), which is in turn overlain by a Piacenzian transgressive succession (Mellere *et al.*, 2005; Roda, 1964; Zecchin *et al.*, 2012). On a larger scale, the TBU corresponds to the Mid-Pliocene Unconformity (MPCU), which is found mainly on the Ionian side of the Calabrian Arc and probably records interference of the arc with the Apulian plate (Zecchin *et al.*, 2015).

## The Belvedere Formation and its cyclicity

The lower Pliocene Belvedere Formation is predominantly an aggradational stack (some hundreds of metres thick) of alternating bioclastic and siliciclastic shallow-marine deposits, which accumulated within half-graben sub-basins between 2·5 km and 5·0 km wide (Zecchin *et al.*, 2004, 2006) (Figs 3 to 5). The latter are bounded by north-east-trending listric growth faults (Fig. 3B), which enabled a pronounced thickness increase in the hanging-walls with respect to the footwalls (Zecchin *et al.*, 2004, 2006).

The most prominent characteristic of the Belvedere Formation is represented by its small-scale cyclicity, which is highlighted by the alternation between shell-rich and shell-poor shallow-marine deposits (Zecchin, 2005) (Fig. 5). Cycles of the Belvedere Formation range between 3 m and 18 m thick, with a typical thickness of 5 to 7 m (Fig. 5). The cyclicity is prominent in the hanging-wall of the synsedimentary normal faults, whereas on the footwalls it is much less apparent (Zecchin, 2005; Zecchin & Caffau, 2012) (Fig. 5). Two types of cycles were identified: Type 1 cycles, composed of storm-dominated shoreface deposits; and Type 2 cycles, composed of large subaqueous dunes in the lower part and by storm-dominated deposits (Zecchin, 2005). Large subaqueous dunes were found mainly in the lower half of the Zinga 3 stratal unit (Fig. 5), and their migration was related to the action of strong tidal currents in tectonically confined areas (Zecchin, 2005). In particular, it is inferred that the activity of the synsedimentary normal faults bounding the half-graben sub-basins in which the Belvedere Formation accumulated (Fig. 3B) have periodically produced depressions that functioned as straits that enhanced tidal currents (Zecchin, 2005). In contrast, relatively high sediment supply

prevented the formation of significant fault scarps during the accumulation of shoreface cycles (Zecchin, 2005). In order to discriminate between WRSs and bedset boundaries, only the Type 1 cycles of Zecchin (2005) (Fig. 5) are considered in the present study.

## METHODS

The basis of this study consists of six measured sections (CBS 1, CBS 2, CBW, MPW, SAL and SMS) documenting both facies and overall stratigraphy of part of the Belvedere Formation

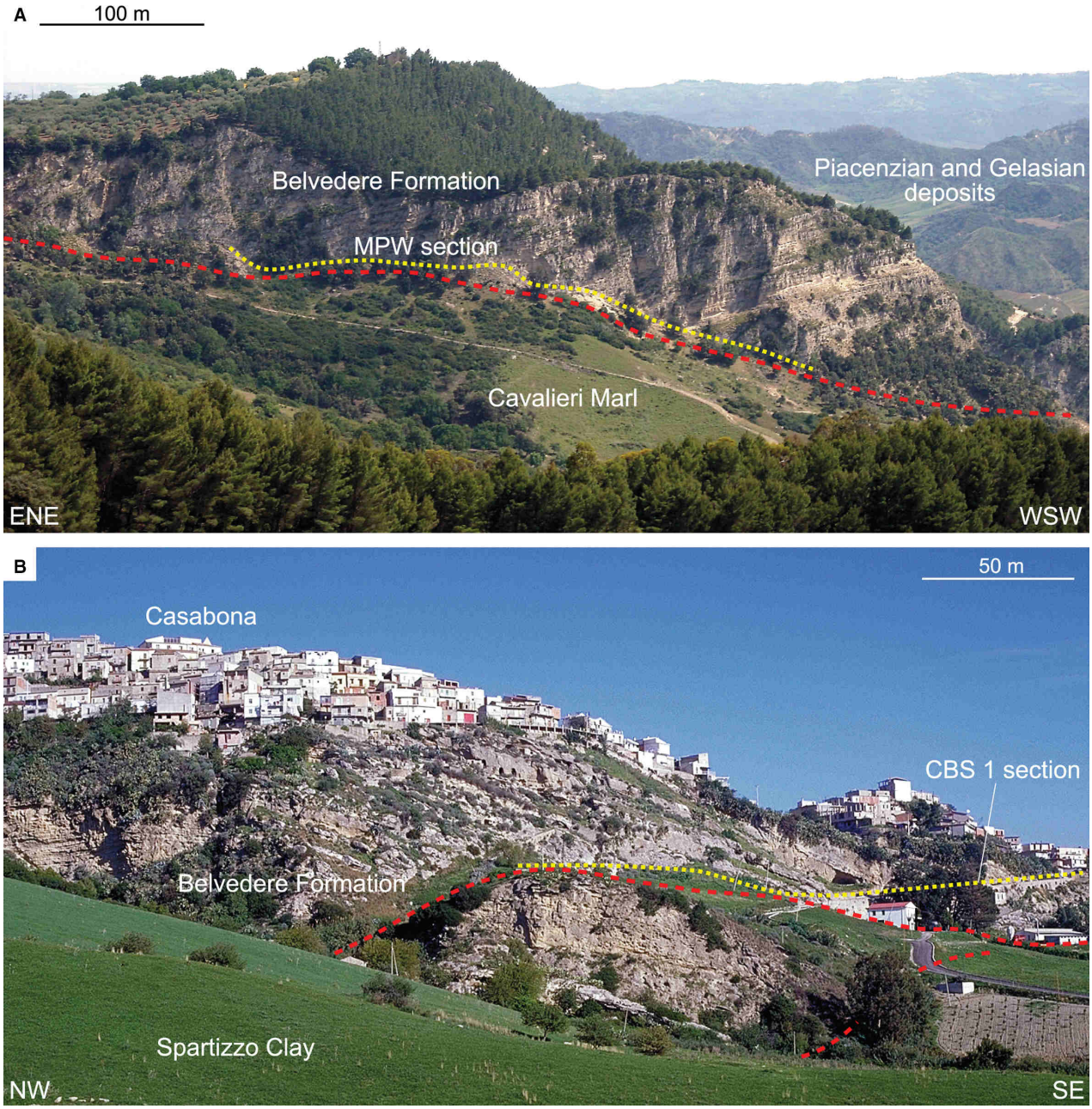


**Fig. 6.** (A) Panoramic view of the West Montagna Piana (MPW) section (see Figs 3A and 5), documenting part of the Belvedere Formation accumulated in the Montagna Piana half-graben (Fig. 3B). The red dotted line indicates the main fault bordering the half-graben. The lower Pliocene Cavalieri Marl was partly eroded, allowing for the study of the sandstone deposits accumulated in the fault-bounded basin. (B) Panoramic view of the South Casabona 1 (CBS 1) section (see Figs 3A and 5), documenting part of the Belvedere Formation accumulated in the Montagna Piana half-graben (Fig. 3B). The red dotted lines correspond to normal faults that were active during accumulation of the Piacenzian Spartizzo Clay.

accumulated in the Montagna Piana and Belvedere half-graben sub-basins and on the Salice horst (Zecchin, 2005; Zecchin & Caffau, 2012; Zecchin *et al.*, 2004) (Figs 3A, 3B, 5 and 6). In order to document the details of the boundaries between some of the characteristic shoreface cycles of the Belvedere Formation (the Type 1 cycles of Zecchin, 2005), new metre-scale details of the sections are shown (Figs 5 and 7 to 10). Excellent exposures (Fig. 6) allowed detailed facies analysis and recognition of key stratal surfaces and facies contacts. This is a standard approach in reconstructing depositional environments, in understanding the significance of the bounding surfaces and ultimately in defining a sequence stratigraphic framework.

Fifty-six sediment samples were collected along the new measured sections (Figs 7 to 10), and approximately 100 g of sediment was taken from each sample for micropalaeontological analyses. The sample aliquots were dried at 50°C for 24 h and then treated with hydrogen peroxide (10% vol) for 12 h, in order to remove the organic matter. Samples were then washed through a 63 $\mu$m mesh and dried. From the corresponding washing residues, 3 g of sediment was separated. All benthic foraminifera present in this amount of sediment were counted and classified following the taxonomic order of Loeblich & Tappan (1987).

Heavy minerals were separated by means of tetrabromohetane ($\rho$ = 2·96 g cm$^{-3}$) and successively counted under a microscope. The micas were not considered because they have specific gravity between 2·6 g cm$^{-3}$ and 3·2 g cm$^{-3}$ and thus cannot be completely separated by treatment with tetrabromohetane; moreover, their platy habit could limit their potential to sink in the liquid.

## FACIES AND SEDIMENTARY ENVIRONMENTS

In the measured sections, five facies composing two facies associations (condensed shallow-marine facies association – A; and siliciclastic shoreface facies association – B) were recognized (Figs 7 to 12). Facies and facies associations are described and interpreted below and summarized in Table 1.

### Condensed shallow-marine facies association (A)

*Facies A1: Conglomerate lag*

Facies A1 is rarely found and consists of a 0·05 to 0·4 m thick very coarse-grained sandstone to granule-grade conglomerate, mostly composed of quartz, with scattered pebbles, pectinid shells and shell fragments (Figs 9A, 10A and 11A). Sand-filled irregular burrows may be found locally in the upper part of the thicker beds forming this facies (Fig. 10A).

The base of Facies A1 typically consists of a laterally extensive erosional surface truncating the deposits of facies association B (Figs 9A, 10A and 11A). Facies A1 is sharply overlain by Facies A2 (Figs 9A, 10A and 11A).

*Facies A2: Shell-rich deposit*

Facies A2 consists of stacked shell beds, each up to 10 cm thick, that form well-cemented tabular units, 0·15 to 2·5 m thick (Figs 7 to 10, 11B, 12A and 13 to 15). Structureless units up to *ca* 1 m thick, containing shells dispersed in a siliciclastic matrix locally mixed with granule-grade shell debris, are also found (Figs 7B, 7D, 10A and 12A). In some cases, shells are more tightly packed in the lower or upper parts of the facies or in both (Figs 7, 8A, 9A and 10B). The siliciclastic component of the matrix varies from fine-grained quartz sandstone to granule-grade quartz conglomerate, with occasional dispersed pebbles. The grain size of the matrix may be relatively uniform from the base to the top of the facies (Figs 7A, 7C, 8B, 8C, 9A and 10A) or may show an upward decrease (Figs 7B, 7D, 8A, 9B and 10B). Facies A2 is generally planar stratified, although local swaley cross-stratification (SCS) and rare trough cross-stratification (TCS) are found (Figs 7 to 10).

Shells (pectinids, ostreids and less commonly venerids), up to 10 cm in size, are disarticulated and in places broken but not abraded (Figs 7 to 10 and 11B). Whole shells are rare. Barnacles are locally common. Shells are usually convex-

**Fig. 7.** Details of the West Montagna Piana (MPW) section (see Fig. 5 for location), documenting facies and wave-ravinement surfaces (WRS) that bound high-frequency sequences composing the Belvedere Formation: (A) WRS at 38 m from the base of the section; (B) WRS at 51 m from the base of the section; (C) WRS at 71 m from the base of the section; (D) WRS at 101 m from the base of the section. HST, highstand systems tract; TST, transgressive systems tract. Grain sizes are as follows: cl = clay; s = silt; vf = very fine; f = fine; m = medium; c = coarse; vc = very coarse; g = granule; pb = pebble; cb = cobble; bd = boulder.

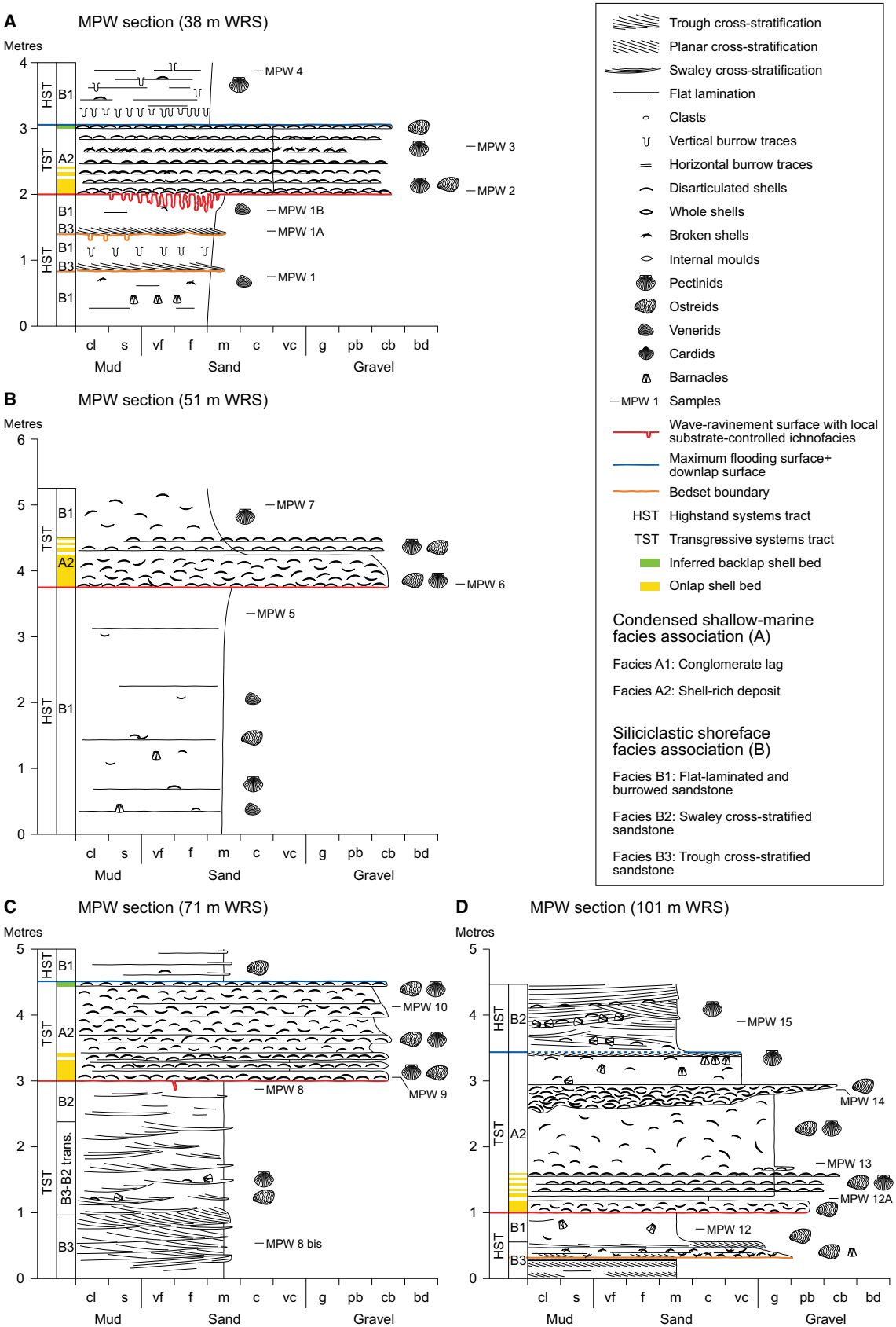
A
MPW section (38 m WRS)
Metres
HST
TST
HST
B1
A2
B1
B3
B1
B3
B1
MPW 4
MPW 3
MPW 2
MPW 1B
MPW 1A
MPW 1
cl s vf f m c vc g pb cb bd
Mud
Sand
Gravel
B
MPW section (51 m WRS)
Metres
TST
HST
B1
A2
B1
MPW 7
MPW 6
MPW 5
C
MPW section (71 m WRS)
Metres
HST
TST
B1
A2
B2
B3-B2 trans.
B3
MPW 10
MPW 8
MPW 9
MPW 8 bis
D
MPW section (101 m WRS)
Metres
HST
TST
HST
B2
A2
B1
B3
MPW 15
MPW 14
MPW 13
MPW 12A
MPW 12
Trough cross-stratification
Planar cross-stratification
Swaley cross-stratification
Flat lamination
Clasts
Vertical burrow traces
Horizontal burrow traces
Disarticulated shells
Whole shells
Broken shells
Internal moulds
Pectinids
Ostreids
Venerids
Cardids
Barnacles
MPW 1 Samples
Wave-ravinement surface with local substrate-controlled ichnofacies
Maximum flooding surface+ downlap surface
Bedset boundary
HST Highstand systems tract
TST Transgressive systems tract
Inferred backlap shell bed
Onlap shell bed
Condensed shallow-marine facies association (A)
Facies A1: Conglomerate lag
Facies A2: Shell-rich deposit
Siliciclastic shoreface facies association (B)
Facies B1: Flat-laminated and burrowed sandstone
Facies B2: Swaley cross-stratified sandstone
Facies B3: Trough cross-stratified sandstone

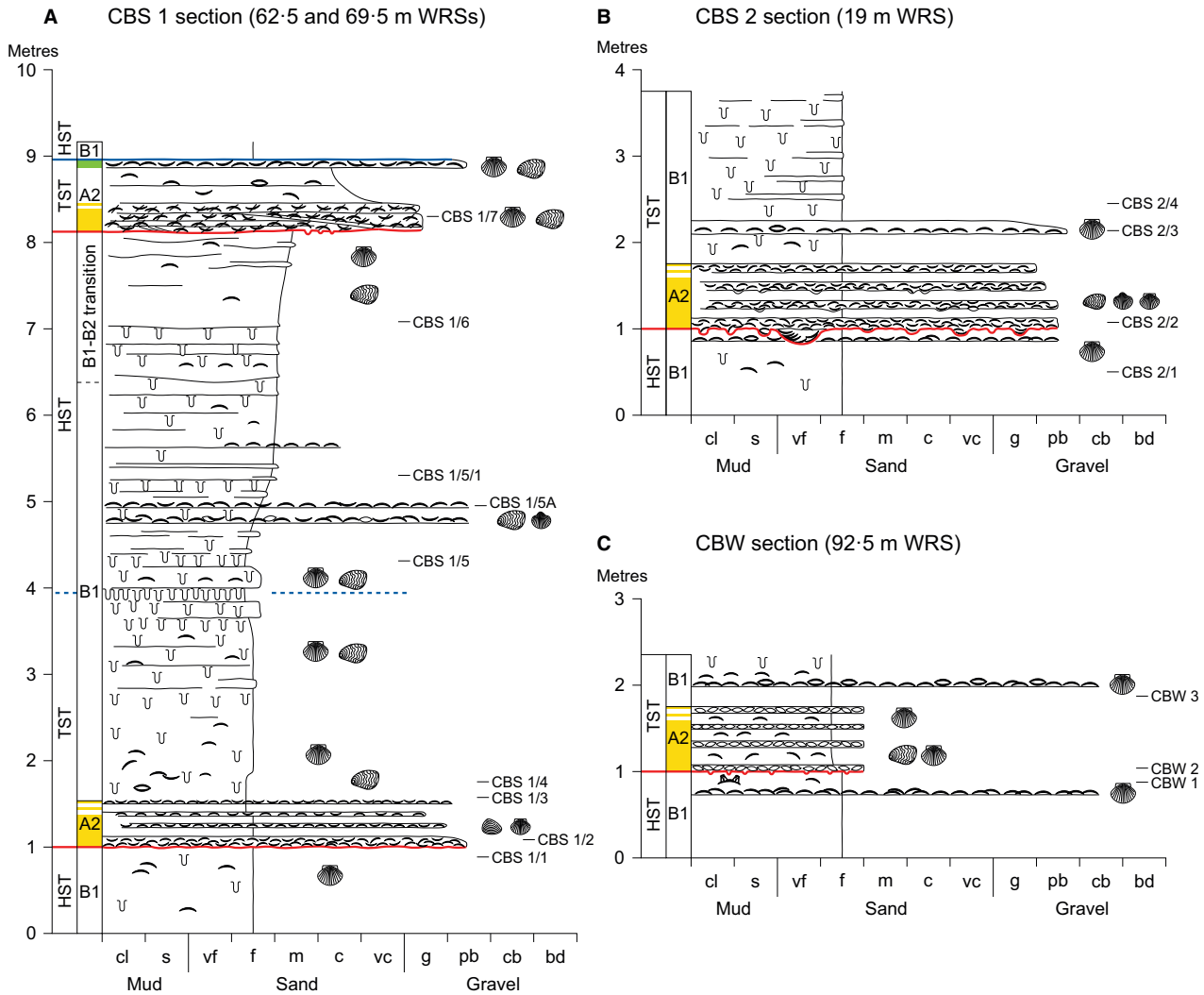


**Fig. 8.** Details of: (A) the South Casabona 1 (CBS 1) section; (B) the South Casabona 2 (CBS 2) section; and (C) the West Casabona (CBW) section, documenting facies and wave-ravinement surfaces (WRS) that bound high-frequency sequences composing the Belvedere Formation (see Fig. 5 for location and Fig. 7 for symbols).

up arranged and less commonly concave-up arranged (Figs 7 to 10, 11B and 13). Edgewise shells are occasionally found. There are rare occurrences of cemented layers containing small internal moulds (Fig. 8C). Overall, larger and robust shells are common in the Facies A2 intervals of the MPW, SMS and TAL sections (Figs 7, 9B, 10, 13 and 14B). Erosional-based, shell-bearing bodies, showing a lenticular shape at outcrop, up to 0·4 m thick and <10 m across, are rarely found (Figs 7D and 12A). Their base is very irregular, with decimetre-scale relief, and the top is flat, whereas their fill consists of very packed oyster shells, usually disarticulated and chaotically arranged, although rare whole shells are present (Figs 7D and 12A).

A substrate-controlled *Glossifungites* ichnofacies in some cases characterizes the base of Facies A2, where the facies directly overlies the deposits of facies association B (Figs 7A, 7C, 8, 9B, 13 and 14). This ichnofacies can be represented by only occasional vertical traces descending up to *ca* 10 cm in the underlying unit (Figs 7C, 8, 13B and 14A) or may consist of a highly burrowed bed up to 30 cm thick, formed by *Thalassinoides*-like traces (Figs 7A, 13A and 14B). The *Glossifungites* ichnofacies is laterally discontinuous and may disappear within a few metres. Vertical burrows may be present also at the base of individual shell beds within the facies (Figs 8B and 10B). Irregular burrows may be dispersed in the beds (Fig. 10A).

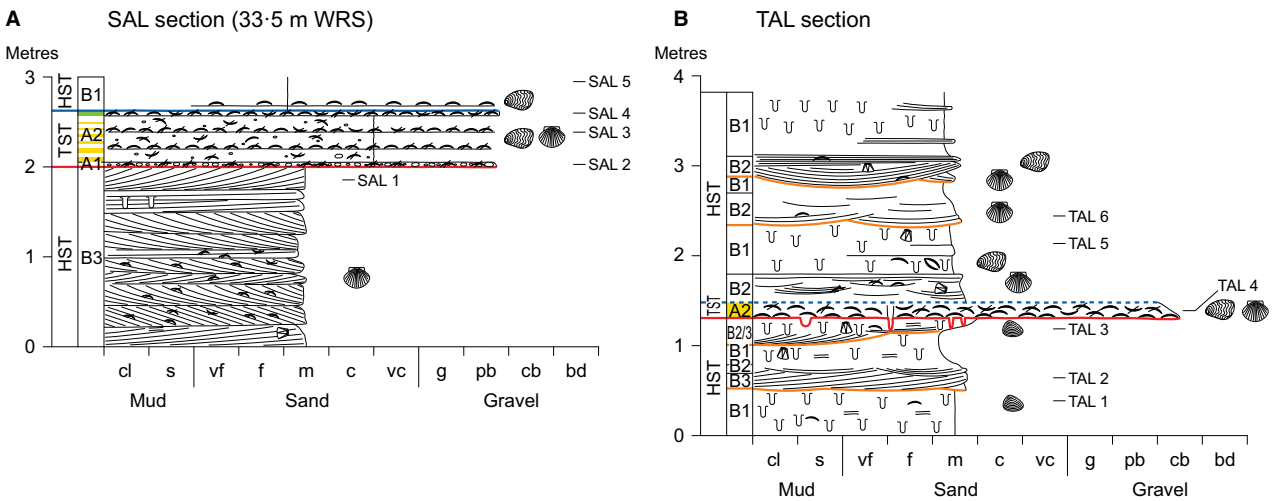


**Fig. 9.** Details of (A) the Salice (SAL) section and (B) the Tallarico (TAL) section, documenting facies and wave-ravinement surfaces (WRS) that bound high-frequency sequences composing the Belvedere Formation (see Figs 3A and 5 for location, and Fig. 7 for symbols).

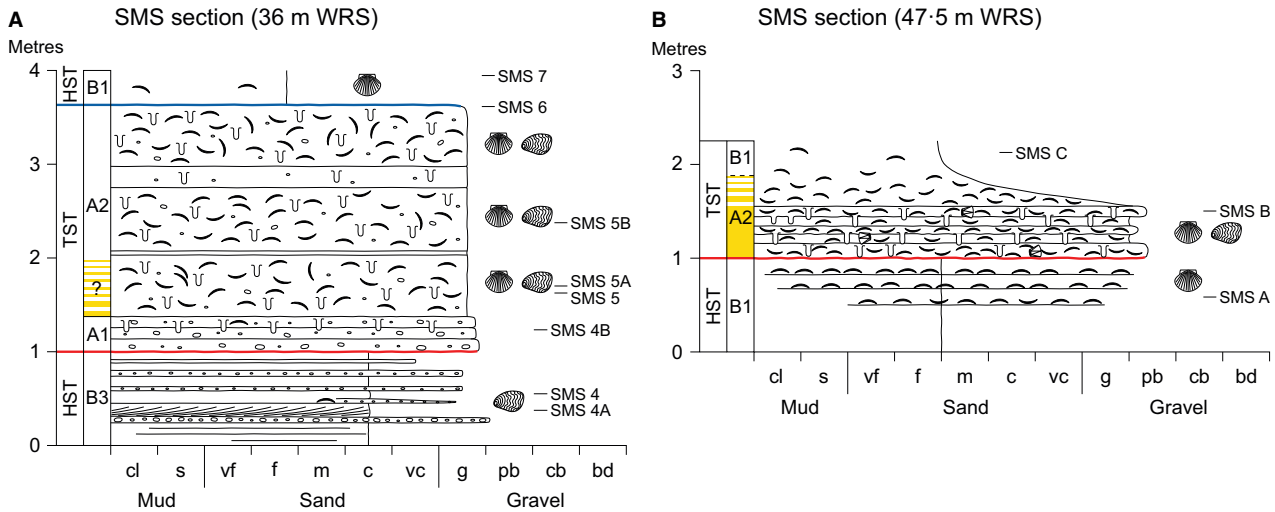


**Fig. 10.** Details of the Santa Maria della Scala (SMS) section, documenting facies and wave-ravinement surfaces (WRS) that bound high-frequency sequences composing the Belvedere Formation (see Fig. 5 for location and Fig. 7 for symbols): (A) WRS at 36 m from the base of the section; (B) WRS at 47·5 m from the base of the section.

Facies A2 sharply overlies Facies A1 or erosionally overlies the deposits of facies association B (Figs 7 to 10 and 13 to 15). The facies is in turn sharply to gradually overlain by Facies B1 or Facies B2 (Figs 7 to 10, 12A, 13A, 14 and 15B).

*Interpretation of facies association A*

The abundance of marine mollusc shells, the relatively coarse grain size and the local occurrence of SCS suggest that the deposits of facies association A accumulated in a shallow-marine environment. The relationship of Facies A1 with an erosional surface truncating, and in turn overlain by, the deposits of facies associations A and B, suggests that this facies is a lag deposit produced by wave erosion, possibly during shoreface retreat, and mostly composed of material reworked from the substrate (Demarest & Kraft, 1987; Hwang & Heller, 2002; Nummedal & Swift, 1987).

In contrast, Facies A2 is rich in intra-basinal skeletal material, most probably accumulated in middle to lower shoreface settings, as indicated

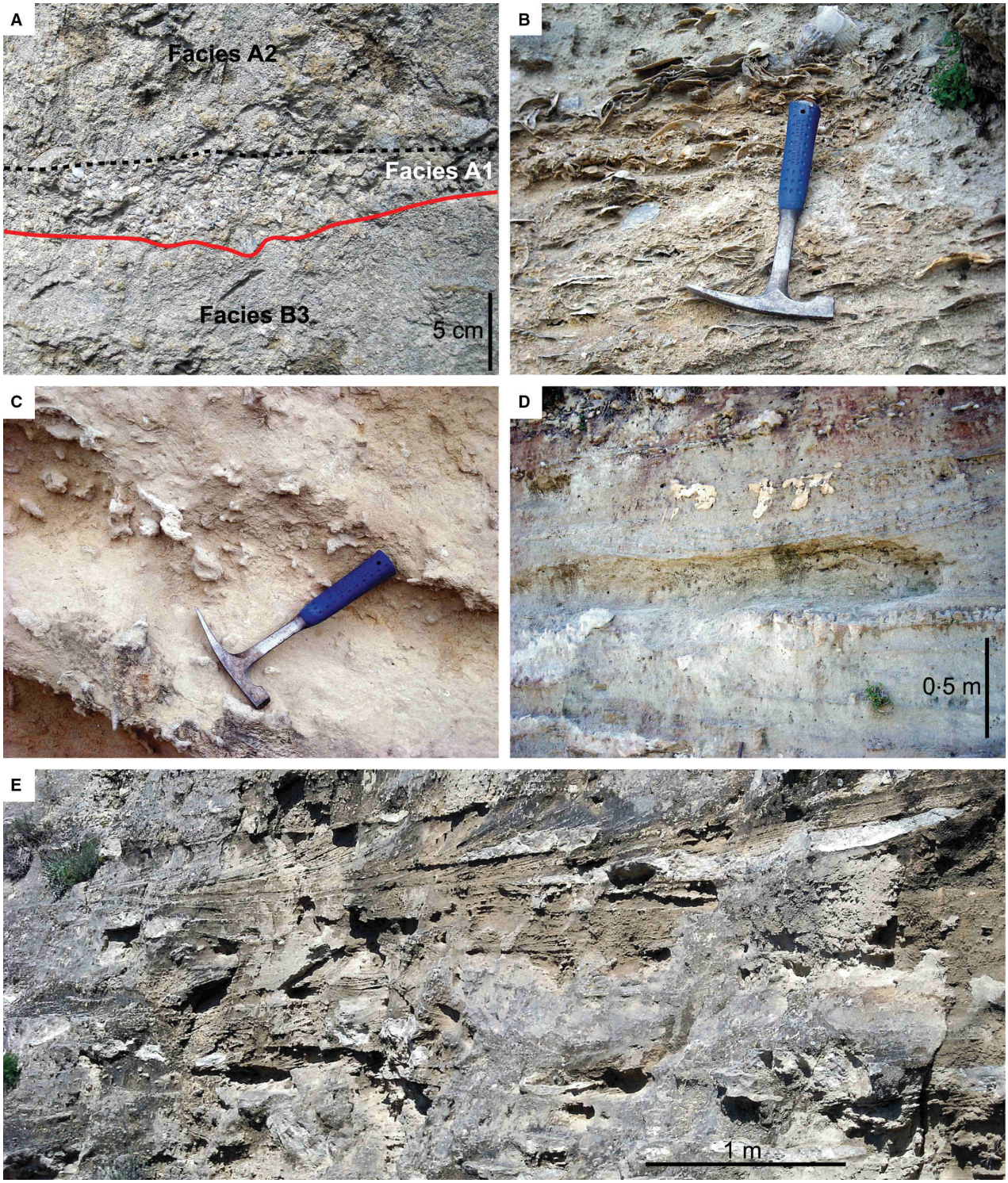


**Fig. 11.** Facies characterizing the shoreface deposits of the Belvedere Formation. (A) Conglomerate lag (Facies A1) in the SAL section (Fig. 9A). (B) Shell-rich deposit (Facies A2) in the MPW section (Fig. 7C). Hammer for scale is 28 cm long. (C) Burrowed sandstone (Facies B1) in the CBS 1 section (Fig. 8A). Hammer for scale is 28 cm long. (D) Swaley cross-stratified sandstone (Facies B2) in the TAL section (Fig. 9B). (E) Trough cross-stratified sandstone (Facies B3) in the SAL section (Fig. 9A).

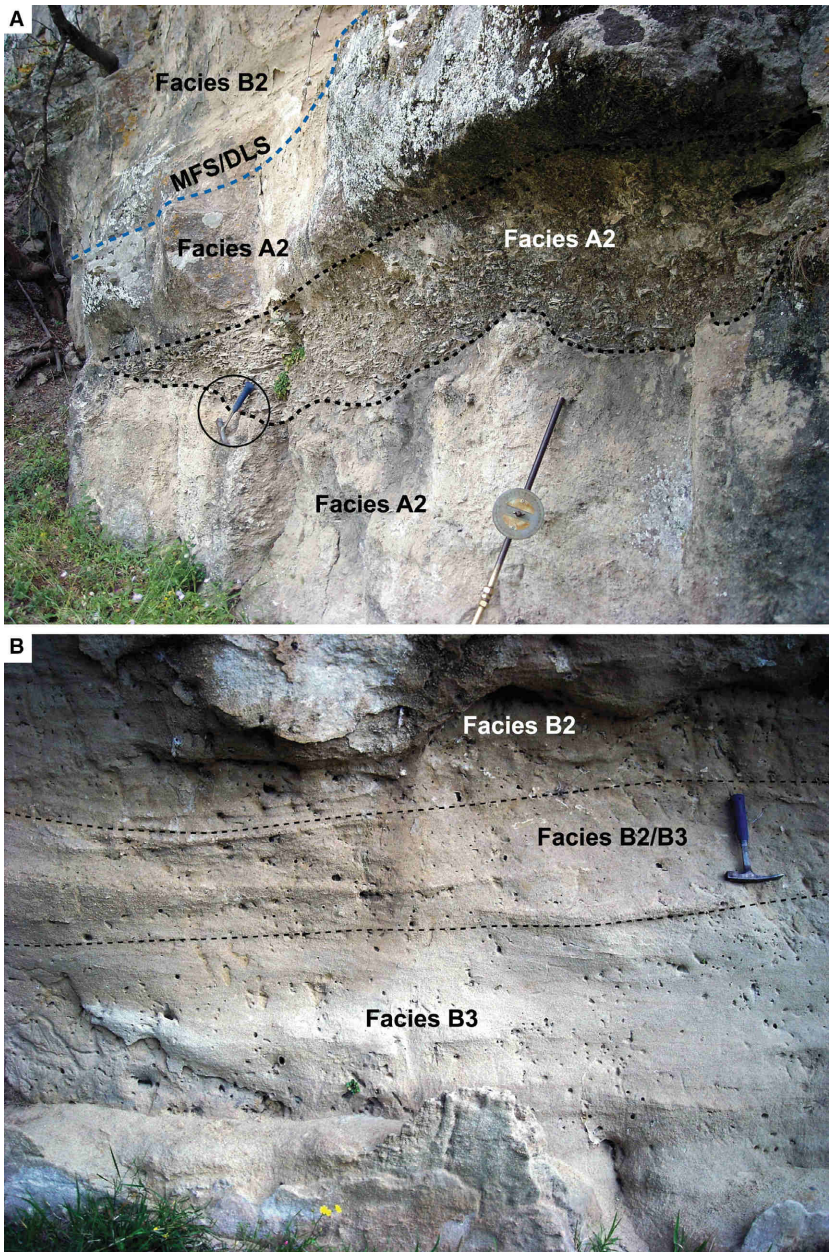


**Fig. 12.** (A) Erosional-based, shell-bearing lens found in Facies A2 (MPW section, Fig. 7D). DLS, downlap surface; MFS, maximum flooding surface. (B) Upward transition from trough cross-stratified sandstone (Facies B3) to swaley cross-stratified sandstone (Facies B2) in the MPW section (Fig. 7C). Facies B2/B3 intermediate deposits are characterized by anisotropic swaley cross-stratification. For both outcrops, hammer for scale is 28 cm long.

**Table 1.** Facies and facies associations of the studied succession.

| Facies association | Facies | Interpretation |
|---|---|---|
| Condensed shallow-marine (A) | A1: Conglomerate lag<br>A2: Shell-rich deposit | Lag deposit in the shoreface<br>Lower to middle shoreface deposit recording low net sedimentation rates |
| Siliciclastic shoreface (B) | B1: Flat-laminated and burrowed sandstone<br>B2: Swaley cross-stratified sandstone<br>B3: Trough cross-stratified sandstone | Low-energy shoreface<br>Storm-dominated middle shoreface<br>Longshore-current-dominated upper shoreface |

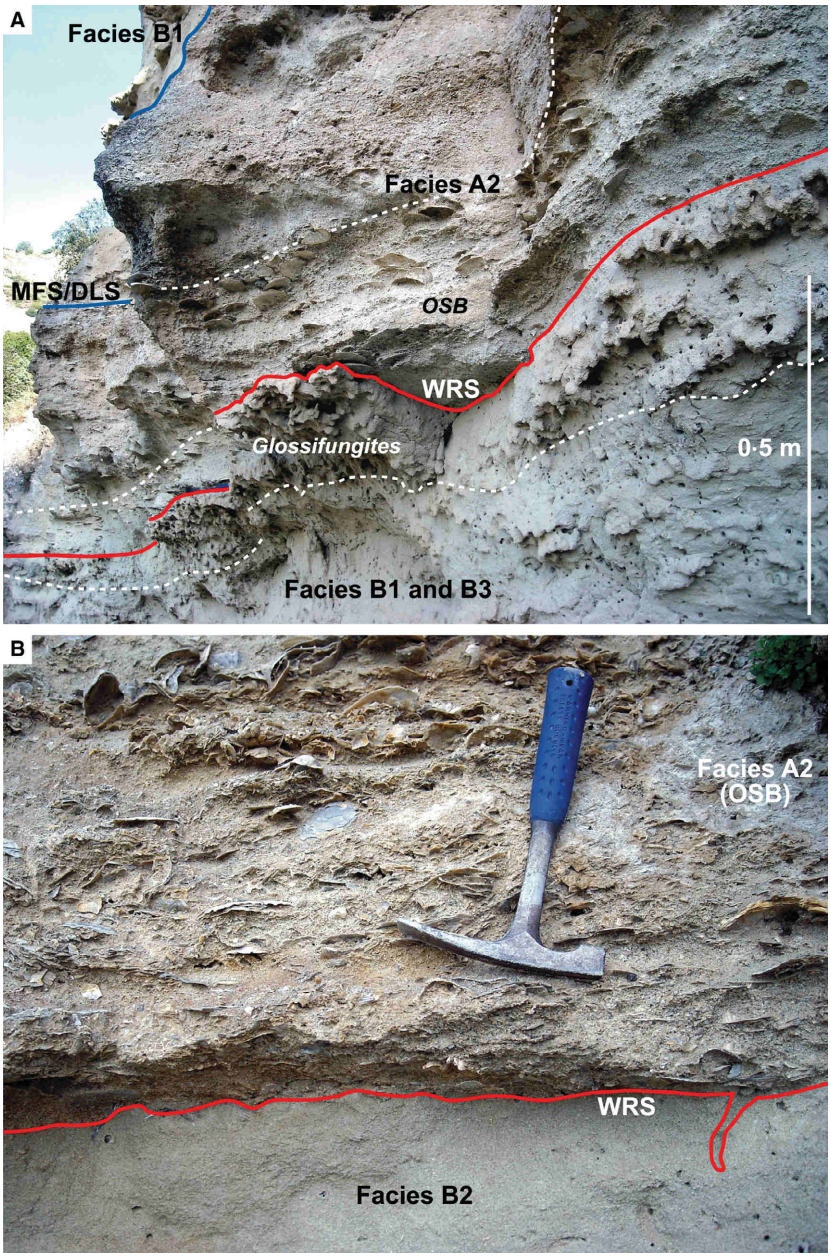


**Fig. 13.** (A) Wave-ravinement surface (WRS) separating two high-frequency sequences in the MPW section (Fig. 7A). Note the dense onlap shell bed (OSB) overlying the WRS and forming part of Facies A2 (shell-rich deposit), and the prominent *Glossifungites* ichnofacies just underlying such a surface. DLS, downlap surface; MFS, maximum flooding surface. (B) Detail of a WRS found in the MPW section (Fig. 7C). Note the OSB overlying the WRS and the small trace descending from that surface. Hammer for scale is 28 cm long.

by the prevailing planar stratification and SCS, which suggest the action of major storm waves (Dott & Bourgeois, 1982; Leckie & Walker, 1982). The facies is probably the product of several storm events (Norris, 1986). The dominance of convex-up shells suggests the occurrence of storm flows that were powerful enough to move large shells, which then settle in the more hydrodynamically stable position (e.g. Cantalamessa *et al.*, 2005; Fürsich & Pandey, 1999). The occasional lenticular shell-bearing bodies (Fig. 7D) are tentatively interpreted as scour and fill features related to exceptional storm events, possibly produced by storm-enhanced rip-currents or more generally by storm-return flows eroding the shoreface (e.g. Hart & Plint, 1995; Leithold & Bourgeois, 1984).

The features of Facies A2, together with the evidence that this deposit directly overlies an erosional surface where Facies A1 is absent, and that its base is marked by a prominent substrate-controlled *Glossifungites* ichnofacies (Figs 7 to 10), suggest accumulation under conditions of sediment bypass during transgressive phases, promoting shell concentration and amalgamation of event beds (Kidwell, 1991; Kondo *et al.*, 1998; Naish & Kamp, 1997a). Facies A2 probably also recorded an increased volume of bivalve

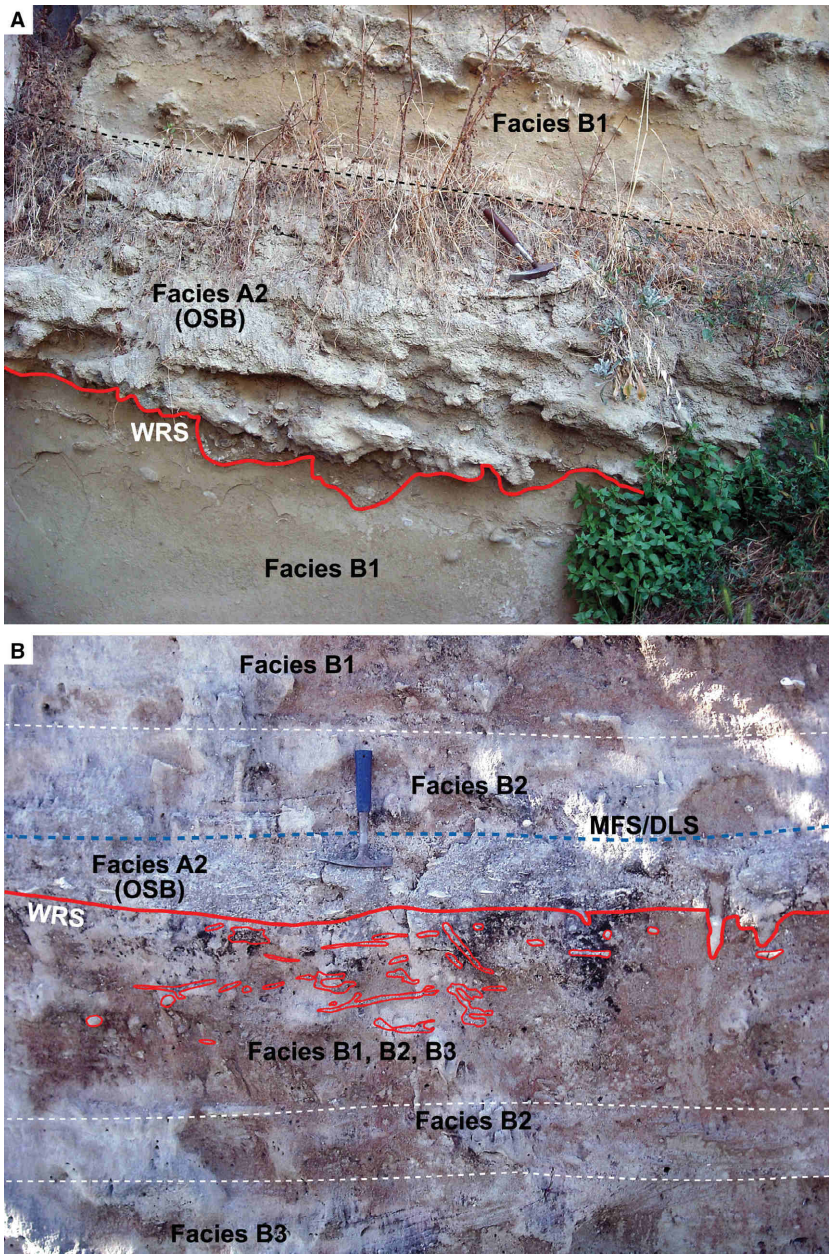


**Fig. 14.** (A) Wave-ravinement surface (WRS) separating two high-frequency sequences in the CBS 2 section (Fig. 8B). Note the onlap shell bed (OSB) corresponding to Facies A2 (shell-rich deposit), and the *Glossifungites* ichnofacies at the WRS. (B) WRS separating two high-frequency sequences in the TAL section (Fig. 9B). Note the relatively deep *Glossifungites* ichnofacies below the WRS. For both outcrops, hammer for scale is 28 cm long. MFS, maximum flooding surface; DLS, downlap surface.

communities favoured by relatively low net sedimentation rates in the shoreface-shelf system during transgression (e.g. Schwarz *et al.*, 2016).

## Siliciclastic shoreface facies association (B)

### *Facies B1: Flat-laminated and burrowed sandstone*

Facies B1 consists of fine to medium-grained quartz sandstone, which may be structureless or may show faint flat lamination, and is locally organized to form decimetre-scale beds (Figs 7 to 10, 11C and 15). The facies thickness reaches *ca* 5 m and shows lateral continuity at outcrop scale.

Shell beds occur up to 10 cm thick and dispersed shells are very common, although their abundance may decrease locally (Figs 7 to 10). Shells consist of up to 10 cm large pectinids and ostreids most commonly disarticulated and convex-up arranged, although whole shells are found locally. Disarticulated and occasionally broken small venerids are rare (Figs 7 to 10). Small barnacles are associated with the mollusc shells.

The bioturbation is very common and usually pervasive, although it may be concentrated to

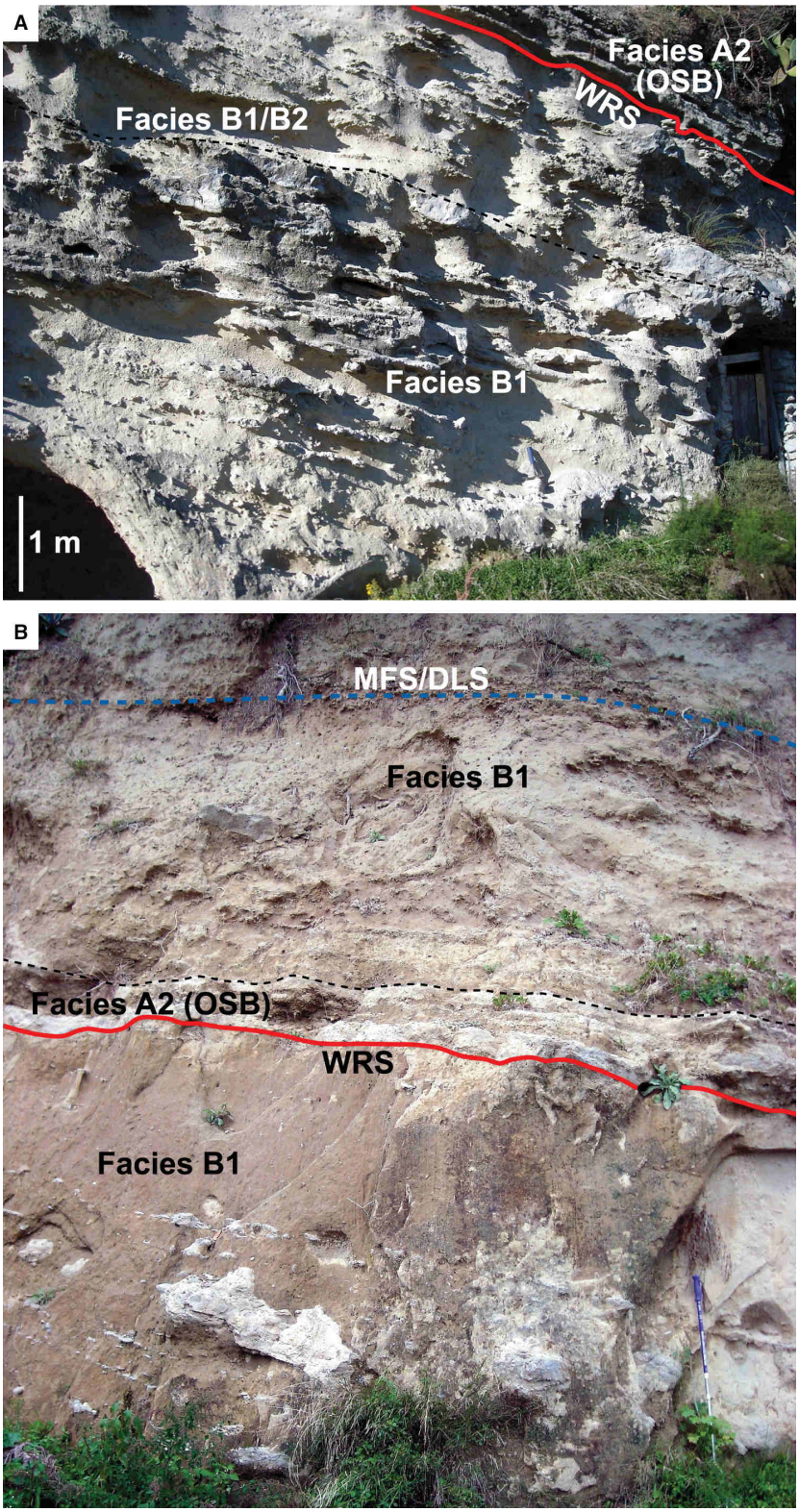


**Fig. 15.** (A) Upper part of the considered detail of the CBS 1 section (Fig. 8A). Note the wave-ravinement surface (WRS) truncating the deposits of facies association B and overlain by a condensed shell bed (onlap shell bed, OSB). (B) Lower part of the considered detail of the CBS 1 section (Fig. 8A; modified from Zecchin & Catuneanu, 2015). Note the OSB (Facies A2) overlying the WRS, and the inferred maximum flooding surface plus downlap surface (MFS/DLS), corresponding to the interval characterized by higher bioturbation level. Pole for scale (below on the right) is 90 cm long.

form decimetre-scale highly burrowed layers or be absent in places (Figs 7A, 8, 9B and 11C). Sand-filled burrows are vertical and occasionally horizontal. Facies B1 may pass upward to or from Facies B2 or Facies B3 (Figs 7A, 7D and 9B); moreover, it may be erosionally overlain by

Facies A2 or may abruptly to gradually overlie Facies A2 (Figs 7, 8, 9A, 10, 13A, 14A and 15B).

*Facies B2: Swaley cross-stratified sandstone*

Facies B2 is up to 1 m thick and is composed of medium-grained quartz sandstone characterized by SCS (Figs 7C, 7D, 9B, 11D, 12B and 14B). Swales are up to 2·5 m wide and 0·25 m deep, and are infilled with concave-up sandstone laminae up to 15° inclined that usually do not show preferential orientation (Fig. 11D). Convex-up arranged pectinid and ostreid shells, and small barnacles, are found occasionally. Bioturbation is uncommon.

Facies B2 may overlie Facies B1 and Facies B3, and may in turn be overlain by Facies B1 (Figs 9B and 14B). Metre-scale alternations between Facies B1 and Facies B2 are locally found (Fig. 9B). Facies B2 may also abruptly overlie Facies A2 or be erosionally overlain by the same facies (Figs 7C, 7D and 13B). Deposits *ca* 1·5 m thick with intermediate characteristics between those of Facies B1 and Facies B2 are found in places; they show flat-lamination, SCS and bioturbation (Figs 8A and 15A). Deposits *ca* 1 m thick with intermediate characteristics between those of Facies B2 and Facies B3 are also found locally; they are characterized by anisotropic SCS, in which swales are filled with sandstone foreset laminae that exhibit unidirectional low-angle (up to 15°) inclination and a tangential basal contact (Figs 7C and 12B). These B2/B3 transitional units grade into Facies B3 downward and into Facies B2 upward (Figs 7C and 12B).

*Facies B3: Trough cross-stratified sandstone*

Facies B3 is 0·1 to 2·0 m thick and usually consists of medium-grained quartz sandstone characterized by TCS, although coarser grain sizes and occasional bioclastic intervals are found (Figs 7A, 7C, 7D, 9, 10A, 11E, 12B and 14B). Sets are 0·1 to 0·25 m thick, and foresets are tangential-based and up to 30° inclined. Planar cross-stratified sets with angular-based foresets are found occasionally (Fig. 9A). In some cases, the sets are alternated, or replaced, by centimetre-scale, granule-grade or pebble-size conglomerate layers, in particular in the upper part of the division (Fig. 10A). Rare silty layers (1 cm thick) are also found (Fig. 7D). Trough cross-stratification shows bidirectional palaeocurrent directions to the north-east and south-west (Zecchin, 2005), although in some locations (i.e. the MPW section, Fig. 7C and D) the palaeocurrents are mostly south-westward directed.

Fossils typically consist of usually broken pectinid or ostreid shells and occasional small barnacles (Figs 7D, 9A and 10A). Bioturbation is uncommon and mainly represented by vertical traces, in places descending from the base of the sets (Figs 7A and 9A).

In the considered outcrops, Facies B3 is locally overlain by Facies B2 or may alternate with Facies B1 (Figs 7A, 7D, 9B and 14B). Facies B3 may be truncated at the top by Facies A1 (Figs 9A and 10A).

*Interpretation of facies association B*

The presence of marine mollusc shells, together with the overall sandy lithology and the occurrence of flat-laminated and swaley and trough cross-stratified facies, suggests that the deposits of facies association B accumulated in a shoreface environment, above fair-weather wave base (Reading & Collinson, 1996).

The features of Facies B1 are indicative of relatively low energy levels in a lower shoreface setting, occasionally swept by storm waves that led to the accumulation of shell beds (Clifton, 2006; Reading & Collinson, 1996). The presence of horizontal burrow traces is also indicative of relatively low energy levels, characteristic of the *Cruziana* ichnofacies (MacEachern & Bann, 2008; Pemberton *et al.*, 1992). Local higher energy levels are indicated by both shell beds, interpreted as event beds, and by vertical burrow traces that characterize the *Skolithos* ichnofacies (MacEachern & Bann, 2008; Pemberton *et al.*, 1992).

The dominance of SCS in Facies B2 indicates higher wave energy than that characterizing Facies B1, suggesting deposition in a middle shoreface setting subjected to oscillatory-dominant flow (Dott & Bourgeois, 1982; Dumas *et al.*, 2005; Leckie & Walker, 1982). The locally observed vertical alternation between Facies B1 and B2 (Fig. 9B) suggests alternating phases dominated by storms and fair weather conditions between lower and middle shoreface settings, probably related to variations in wave height, in turn possibly linked to periodic variations in storm energy (e.g. Hampson, 2000; Hampson & Storms, 2003).

Facies B3 is inferred to have accumulated in a high-energy environment characterized by the migration of three-dimensional and locally two-dimensional dunes in upper shoreface settings, producing trough and planar cross-stratification (Clifton, 1981, 2006; Hart & Plint, 1995; Massari & Parea, 1988). The observed

palaeocurrent directions are inferred to be parallel to the palaeoshoreline trend (Zecchin, 2005), and therefore the dunes probably migrated within longshore troughs. Cross-stratified deposits similar to those characterizing Facies B3 were observed also in tide-dominated contexts (e.g. Chiarella & Longhitano, 2012; Longhitano *et al.*, 2014). However, due to the absence of mud drapes and segregated siliciclastic/bioclastic laminae, tidal control is ruled out and a wave-dominated setting is inferred. The thin conglomerate layers are most likely to be related to storm waves that redistributed the coarsest sediment (e.g. Leithold & Bourgeois, 1984). The occasional silty layers were produced by the settling of fine-grained sediment either resuspended by storm waves or introduced by floods (Clifton, 2006). The locally observed alternation between Facies B1 and Facies B3 (Fig. 7A and D), with the local interposition of Facies B2 (Fig. 9B), suggests periodic variations in the intensity of longshore currents, and in general of the environmental energy, in the upper shoreface or at the transition between the upper and the middle shoreface (Clifton, 2006; Johnson & Baldwin, 1996).

The deposits with intermediate characteristics between those of Facies B1 and Facies B2 (Fig. 8A), and of Facies B2 and Facies B3 (Fig. 7C), suggest deposition in settings intermediate between the lower and middle shoreface, and between the middle and upper shoreface, respectively. In particular, the anisotropic SCS characterizing Facies B2/B3 intermediate deposits (Fig. 12B) is inferred to reflect the action of combined flows having both oscillatory and unidirectional components (Datta *et al.*, 1999; Dumas & Arnott, 2006).

In the Belvedere Formation, Facies B1 to B3 are rarely observed to form a complete regressive shallow-marine succession typified by a shallowing-upward trend (Zecchin, 2005; Zecchin & Caffau, 2012). The succession formed by facies association B is more commonly incomplete and bounded at the base and at the top by the deposits of facies association A (Figs 7 to 10). Moreover, the stacking of Facies B1 to B3 shows, in some cases, an opposite trend in specific sections; for example, the observed upward transition from Facies B3 to Facies B2 in the MPW section (Figs 7C and 12B) is inferred to reflect a deepening-upward trend from upper to middle shoreface and/or a variation of the wave/current regime (e.g. Zecchin, 2005).

## HIGH-FREQUENCY SEQUENCES

### Features of the bounding surfaces

The erosional contact between the deposits of facies associations B (below) and A (above), overlain by a lag (Facies A1) or a shell-rich deposit (Facies A2), and marked by a *Glossifungites* ichnofacies (Figs 7 to 10 and 13 to 15), has the features of a wave-ravinement surface (WRS) generated by the action of waves in the shoreface during transgressive episodes (Demarest & Kraft, 1987; Nummedal & Swift, 1987; Swift, 1968). However, in the study area, these surfaces never erode back-barrier or continental deposits, and the maximum observed facies change across them is from upper (below) to lower (above) shoreface (Figs 7 to 10).

These surfaces are probably the result of enhanced wave action on the sea floor. It is known that the mechanisms leading to the formation of stratal discontinuities in lower shoreface deposits, which may include minor relative sea-level changes, variations in wave regime and sediment supply changes, are very difficult to discriminate only on the basis of a vertical facies succession (Hampson, 2000; Storms & Hampson, 2005). However, discontinuities related to variations in wave regime tend to disappear landward, whereas those related to minor relative sea-level changes are well recognizable in the upper shoreface, foreshore and back-barrier deposits (Storms & Hampson, 2005). The formation of transgressive surfaces may also be related to sediment supply changes, which can generate high-frequency sequences (Catuneanu & Zecchin, 2013; Catuneanu *et al.*, 2009).

The evidence of deepening across some of the studied erosional surfaces from upper to lower shoreface (Figs 7A, 7D, 9A and 10A), therefore, points to either relative sea-level changes and/or sediment supply changes controlling the formation of such surfaces and cyclicity. A relatively large-scale control is suggested by the observed lateral continuity of the surfaces in the half-graben sub-basins within which the Belvedere Formation accumulated (Zecchin, 2005). Another clue is provided by the presence of large subaqueous dunes within the cycles of the Belvedere Formation (Fig. 5), the migration of which was associated with stages of minor relative sea-level rise (Zecchin, 2005).

Due to their erosional character and association with lags, shell-rich deposits and *Glossifungites* ichnofacies, the studied surfaces are

therefore still considered as distal parts of WRSs rather than maximum regressive surfaces (MRS) (Figs 7 to 10 and 13 to 15). In some instances, deposits accumulated at similar water depth both below and above the WRSs, or even slightly shallower deposits above, are observed (Figs 7B, 8 and 10B); these anomalous situations may be justified by either very modest (metre-scale) relative sea-level changes or the removal of more proximal facies of the underlying succession by wave action during transgression. The observed association of the surfaces with condensed shell-rich deposits, typical of transgressive trends and the evidence that the succession overlying the surfaces usually records an upward decrease in environmental energy (Figs 7 to 10), rule out their interpretation as regressive surfaces of marine erosion (RSME) bounding the base of the forced regressive portion of the shoreface. Moreover, RSMEs tend to be cryptic within fully shoreface deposits (Catuneanu, 2006), whereas they are well recognizable only in more distal settings, between shelf mud and sharp-based shoreface sands. The reworking of the innermost part of the RSMEs and of the forced regressive shoreface deposits by the WRSs cannot be ruled out.

The studied WRSs are planar to irregular, with centimetre to decimetre-scale relief (Figs 13 to 15), and show lateral continuity at outcrop scale, whereas their updip and downdip terminations are not visible due to outcrop limitations. Because the WRSs separating facies associations A and B are the most prominent surfaces in the studied succession (Figs 13 to 15), they represent the best choice as boundaries of the cycles composing the Belvedere Formation. Since these boundaries are inferred to be associated with shoreline dislocations, the cycles of the Belvedere Formation meet the definition of high-

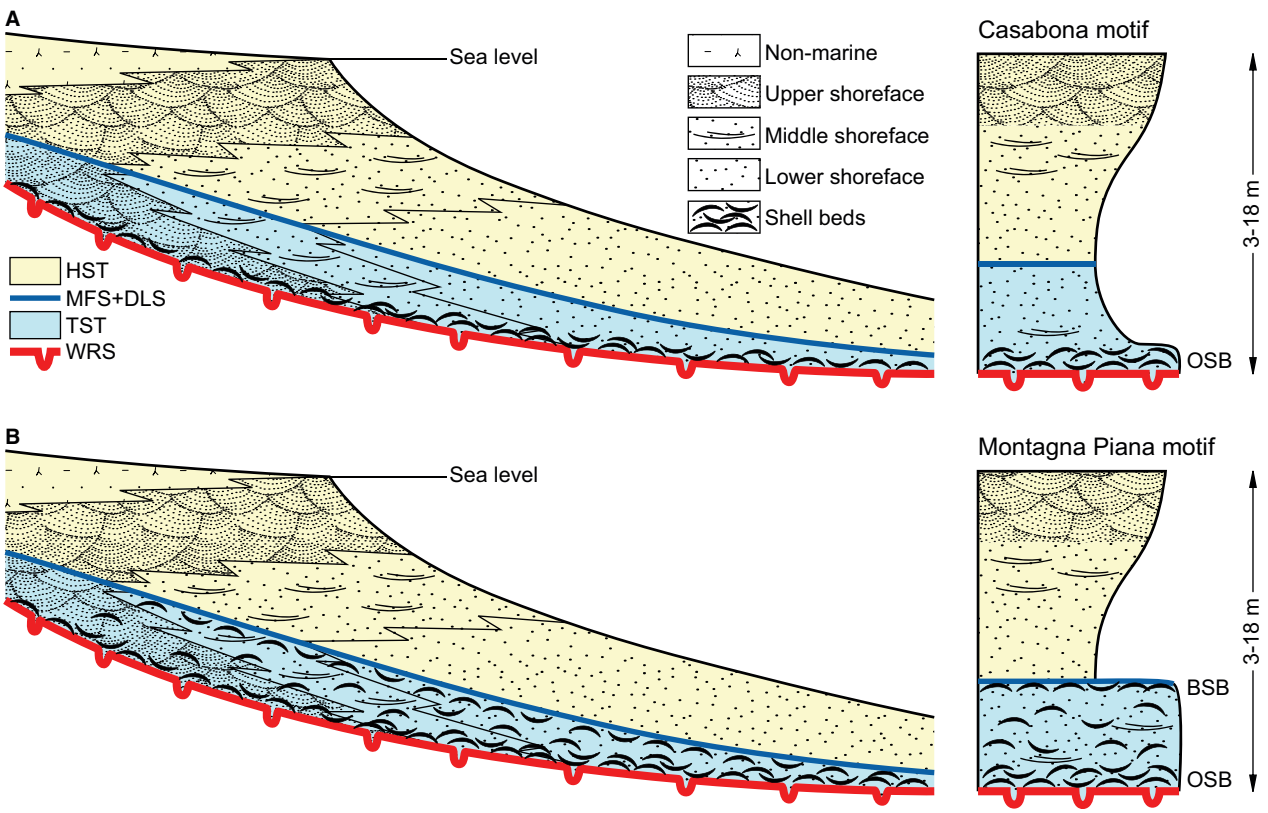


**Fig. 16.** Characteristic shoreface sequence motifs found in the Belvedere Formation. (A) The Casabona motif, which is common in the Casabona (CBS 1, CBS 2 and CBW) sections, is characterized by a gradational contact between the shell-rich transgressive deposits and the overlying shoreface sandstones. (B) The Montagna Piana motif, which is common in the West Montagna Piana (MPW) section, is characterized by a sharp contact between the shell-rich transgressive deposits and the overlying shoreface regressive sandstones. BSB, backlap shell bed; DLS, downlap surface; HST, highstand systems tract; MFS, maximum flooding surface; OSB, onlap shell bed; TST, transgressive systems tract; WRS, wave-ravinement surface.

frequency sequences following Catuneanu & Zecchin (2013) and Zecchin & Catuneanu (2013).

### Architecture of the high-frequency sequences

The relationship of the shell-rich deposits (Facies A2) with lags (Facies A1) and with WRSs suggests that they are transgressive. Facies A2, or at least its densely packed lower part, is inferred to represent an onlap shell bed (OSB; Kidwell, 1991; Naish & Kamp, 1997a; Kondo *et al.*, 1998), mantling the WRS or a transgressive lag (Figs 7 to 10 and 13 to 15) and accumulated after repeated storm reworking during transgression. Facies A1 and A2 therefore form part or the whole transgressive systems tract (TST) of the high-frequency sequences (Figs 7 to 10).

Two characteristic shoreface sequence motifs, based on the architecture of the transgressive deposits, were recognized: the Casabona motif, typical but not exclusive of the Casabona (CBS 1, CBS 2 and CBW) sections and the Montagna Piana motif, typical but not exclusive of the west Montagna Piana (MPW) section (Fig. 16A and B).

Where the contact between Facies A2 (below) and the shell-poor Facies B1 (above) is gradational, the TST probably continues in the lower part of the latter, and the OSB is represented by the whole Facies A2 (Casabona motif; Figs 7B, 8, 10B and 16A). An example of the Casabona motif is provided by the detail of the CBS 1 section (middle part), where the maximum flooding surface (MFS) is picked at an interval characterized by the highest level of bioturbation, *ca* 3 m above the basal WRS (Figs 8A and 15B). The MFS, inferred to approximate the downlap surface (DLS) at the base of the prograding clastic wedge (Zecchin & Catuneanu, 2013), is overlain by a gradually coarsening-upward and shallowing-upward succession *ca* 4 m thick inferred to represent the highstand systems tract (HST) of the sequence (Figs 8A and 15A). The falling-stage systems tract (FSST) and the lowstand systems tract (LST) are not identifiable in any of the examples (Figs 7 to 10). Both the FSST and the LST may have been deposited further seaward if the studied high-frequency sequences were controlled by cycles of minor relative sea-level change, whereas they would not have formed in the case of cycles controlled by changes in sediment supply. The lack of FSSTs may also be explained by stages of sea-level fall being outpaced by rapid fault-controlled subsidence within the half-graben sub-basins within which these sequences accumulated, resulting in continuous relative sea-level rise with varying rates (Zecchin, 2005; Zecchin *et al.*, 2006).

In contrast, where the contact between Facies A2 (below) and Facies B1 or B2 (above) is sharp, Facies A1 plus Facies A2 are inferred to represent the TST, whereas the deposits of Facies association B would represent the HST of the high-frequency sequence (Montagna Piana motif; Figs 7A, 7C, 7D, 8A, 9, 10A and 16B). The OSB is probably represented by the denser lower part of Facies A2, which in this case is usually relatively thick (Figs 7A, 7C, 7D, 8A, 9, 10A, 13 and 14B). The upper part of Facies A2, occasionally showing a prominent shell bed (Figs 7A, 7C, 8A and 9A), might represent the landward equivalent of the backlap shell bed (BSB; Kidwell, 1991), which starts to develop near the end of transgressive episodes and represents a condensed section (Zecchin & Catuneanu, 2013). Typical BSBs usually accumulate in more distal locations than OSBs as the result of sediment starvation and condensation on the shelf (Kidwell, 1991); whereas in the present case they are similar to the OSBs, although thinner. The MFS commonly lies within the BSB (Zecchin & Catuneanu, 2013); however, given the modest thickness of the inferred BSBs, such a surface is considered to approximate the DLS at the top of Facies A2 (Figs 7A, 7C, 7D, 8A, 9, 10A, 13A and 14B). The reader is referred to Zecchin & Catuneanu (2013) for a complete review of the relationships between condensed shell beds, sequence stratigraphic surfaces and facies contacts.

Shell richness in the deposits between the OSB and the inferred BSB in the Montagna Piana motif (Figs 7A, 7C, 7D, 8A, 9 and 10A) has probably been favoured by overall relatively low net sedimentation rates during transgression, which led to an increase in bivalve communities (e.g. Schwarz *et al.*, 2016), as well as by a higher amalgamation of event beds with respect to the HST. In few instances, however, OSBs are not clearly identifiable within Facies A2 (Figs 9A and 10A).

The observed upward transition from Facies B3 to Facies B2 in the MPW section (Figs 7C and 12B) is interpreted to represent a deepening-upward trend from upper to middle shoreface and suggests that, in some cases, facies association B is also transgressive. In such cases, therefore, the regressive part of the sequences was truncated by the WRS, resulting in sequences composed of only the TST (e.g. Di

Celma & Cantalamessa, 2007) (Fig. 7C). Asymmetrical sequence architectures dominated by the TST correspond to the '*T cycle*' architecture of Zecchin (2007), whereas nearly symmetrical architectures, such as in the case of the CBS 1 section (Fig. 8A), correspond to the '*T–R cycle*' architecture of Zecchin (2007). The accumulation of these relatively thick TSTs, in part composed of terrigenous deposits of facies association B, requires a relatively high sediment supply in the shoreface during transgression, which was able to partly compensate for the rate of accommodation creation (Zecchin, 2007).

Overall, the architectures of the high-frequency sequences composing the Belvedere Formation, in particular the *T cycle* and *T–R cycle* architectures, are similar to those illustrated in other Neogene and Quaternary cyclic shallow-marine successions, such as those of the Plio-Pleistocene of the Wanganui Basin, New Zealand (Abbott, 1997; Abbott & Carter, 1994; Naish & Kamp, 1997a; Saul *et al.*, 1999), the Pleistocene of the Canoa Basin, Ecuador (Di Celma *et al.*, 2005) and the Miocene of the northern Chile (Di Celma & Cantalamessa, 2007). In all of these cases, the origin of the cyclicity was associated with glacio-eustasy.

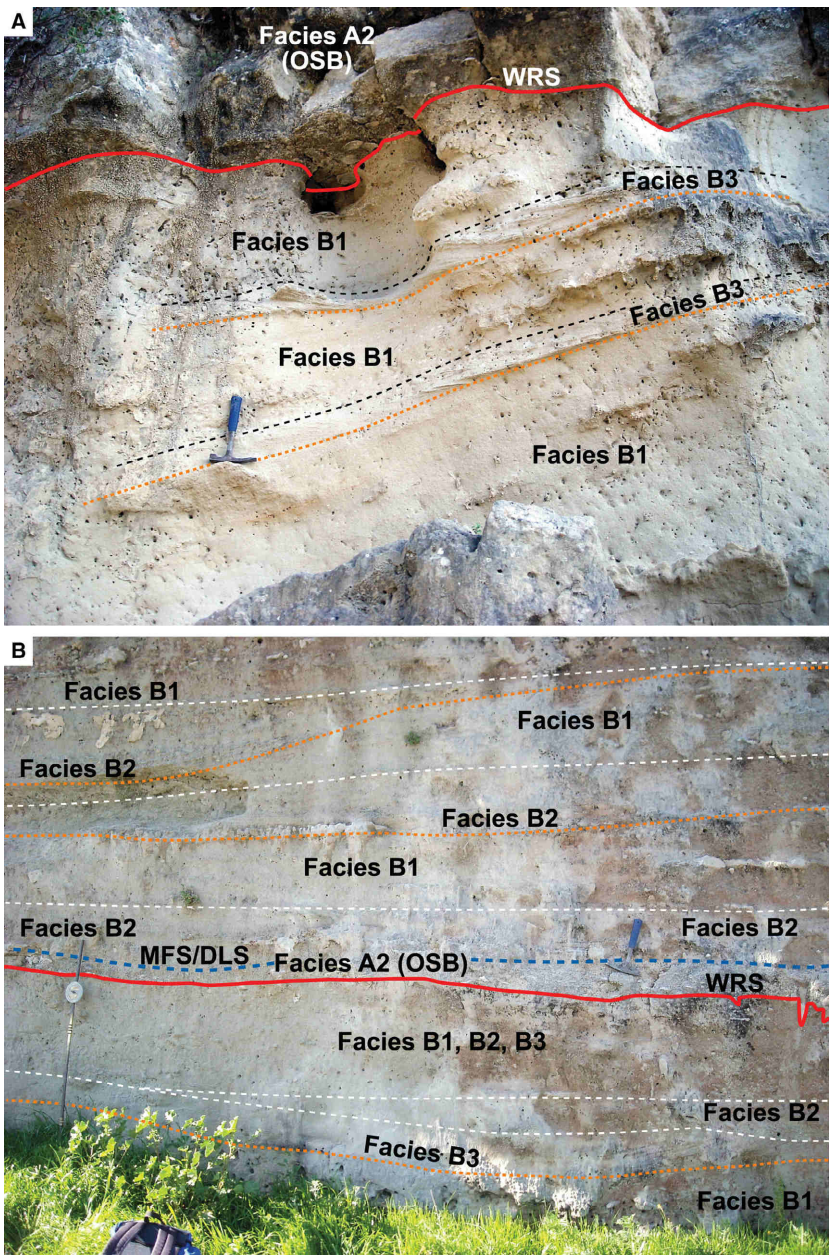


**Fig. 17.** (A) Two erosional surfaces (orange dotted lines) bounding bedsets in transitional upper/middle shoreface deposits of the MPW section (Fig. 7A). Bedsets are highlighted by the alternation between Facies B3 and Facies B1. Note the wave-ravinement surface (WRS) separating two high-frequency sequences and overlain by an onlap shell bed (OSB). (B) Erosional surfaces (orange dotted lines) bounding metre-scale bedsets in transitional upper/middle shoreface deposits (below the WRS) and middle shoreface deposits (above the WRS) of the TAL section (Fig. 9B). Bedsets are highlighted by the alternation between Facies B3, B2 and B1 (below the WRS), or between Facies B2 and B1 (above the WRS). DLS, downlap shell bed; MFS, maximum flooding surface.

### Bedsets and bedset boundaries

The discrimination between discontinuities formed independently of shoreline shifts (i.e. bedset boundaries; Catuneanu & Zecchin, 2013; Zecchin & Catuneanu, 2013) and those related to minor shoreline shifts (i.e. surfaces bounding high-frequency sequences) is difficult, especially in sediments accumulated in lower shoreface or more distal settings, and in the absence of well-exposed dip sections (Storms & Hampson, 2005). In this case study, because the prominent surfaces separating facies association B (below) from facies association A (above) are classified as WRSs which bound high-frequency sequences (Figs 7 to 10 and 17), bedset boundaries are less evident in the field. In particular, bedset boundaries separate bedsets within systems tracts and are recognizable only occasionally in the studied sequences on the basis of variations in the degree of amalgamation of event beds.

Bedsets accumulated in middle shoreface settings are well recognizable in the upper part of the Tallarico section (Figs 9B and 17B); they consist of metre-scale cycles bounded at the base by erosional surfaces and showing an upward decrease in the degree of amalgamation of event beds. The lower part of the bedsets consists of amalgamated SCS (Facies B2), whereas their upper part is composed of burrowed sandstones (Facies B1). An erosional surface marked by a *ca* 30 cm deep *Glossifungites* ichnofacies and overlain by a 15 cm thick shell bed (Facies A2) is interpreted as a WRS separating two high-frequency sequences (Figs 9B and 17B). In turn, this WRS represents the base of one of the bedsets.

Present data also indicate that the upper shoreface and transitional upper/middle shoreface deposits locally consist of decimetre-scale (up to 1 m thick) cycles that can be referred to as bedsets bounded by erosional discontinuities; this observation is exemplified by the occasional alternation between Facies B3 and Facies B1, with the local interposition of Facies B2 (Figs 7A, 7D and 17A). The erosional discontinuities, at the base of Facies B3, may be marked by a less prominent *Glossifungites* ichnofacies, represented by small vertical burrows (Fig. 7A). Bedsets involving Facies B3 are inferred to be generated by periodic variations in the intensity of longshore currents (see *Facies and sedimentary environments* section).

In contrast to all other examples of cycles involving Facies B2 and B3, the upward transition from Facies B3 to Facies B2 found in the MPW section (Figs 7C and 12B) is *ca* 3 m thick and testifies to an overall upward change of depositional processes (i.e. from longshore currents to oscillatory-dominant flow), rather than a decimetre-scale alternation between these facies. As stated earlier, it is inferred that this interval represents a gradual upward deepening accompanied by shoreline transgression, and therefore it would consist of part of the TST of a high-frequency sequence rather than a bedset (Fig. 7C).

## MICROPALAEONTOLOGICAL ANALYSIS

In the samples analysed, the number of specimens for 3 g of sediment is low and some assemblages are completely reworked, as is expected in shallow-marine sediments. However, the micropalaeontological analysis has allowed for identification of specific assemblages of benthic micro-foraminifera within facies (Table 2).

### Benthic foraminifera assemblages in Facies A1 and A2

*Description*

The general occurrence of abraded and fragmented tests indicates that a reworked assemblage (R assemblage; Fig. 18 and Table 2) is present in the conglomerate lags of Facies A1. In contrast, Facies A2 is characterized by three types of assemblages. The first type is dominated by *Quinqueloculina laevigata*, *Quinqueloculina seminulum* and *Quinqueloculina* sp., and occasional *Triloculina* sp., whereas other species are infrequent (Q assemblage; Fig. 18 and Table 2). It should be noted that this assemblage is associated with shell beds consisting of relatively small shells, such as those found in the CBS 1, CBS 2 and CBW sections (Fig. 8).

The second type of benthic foraminifera assemblage of Facies A2 consists of only few abraded, reworked specimens (R assemblage; Fig. 18 and Table 2). It is associated with shell beds composed of large and robust shells, such as those of the MPW, SMS and TAL sections, and occasionally with shell beds composed of broken shells, such as in the upper part of the CBS 1 section (Fig. 8A).

The third type of assemblage of Facies A2 is found only in the SAL section (Fig. 9A); it consists of relatively abundant *Ammonia* spp., *Elphidium crispum* and *Elphidium macellum* (AE assemblage; Fig. 18 and Table 2). This

assemblage is associated with bivalve shells that are commonly broken (Fig. 9A).

*Interpretation*

Due to the presence of only reworked specimens, the assemblage found in Facies A1 indicates high-energy conditions during the formation of the WRS at the base of the lag. Based on the occurrence of *Quinqueloculina* spp., the Q assemblage found in Facies A2 is inferred to indicate relatively moderate to high-energy levels in a lower shoreface environment (Samir *et al.*, 2003; Serandrei-Barbero *et al.*, 2004). However, the highest energy levels in Facies A2 are thought to be associated with the R assemblage, which is dominated by reworking. This fits with the observed coarser skeletal material found in the intervals of Facies A2 typified by this assemblage. Facies A2 intervals characterized by large shells and by the R assemblage are therefore inferred to document the most energetic storm events in middle to lower shoreface settings.

The presence of *Ammonia* spp. and *Elphidium* spp., which are typical of shallow-water settings (Donnici & Serandrei-Barbero, 2002; Mendes *et al.*, 2004; Naish & Kamp, 1997b), together with the inferred overall high environmental energy that favours the breaking of the bivalve shells, suggests a relatively proximal depositional setting for the AE assemblage found in Facies A2, possibly in the uppermost part of the middle shoreface. This relative proximity to the shoreline may explain the absence of *Quinqueloculina* spp. which usually lives in slightly more distal settings (Naish & Kamp, 1997b).

### Benthic foraminifera assemblages in Facies B1 and B2

*Description*

Facies B1 and B2 contain a similar benthic foraminifera assemblage which is characteristic for all sections. The specimens are well-preserved, indicating limited transport. The assemblage consists of *Ammonia* spp., *Elphidium* spp. plus locally common *Asterigerinata planorbis*, *Florilus boueanum* and *Cibicides lobatulus* (AE assemblage; Fig. 18 and Table 2). In rare instances, and where Facies B1 is associated with Facies B3 (MPW section, 101 m WRS, Fig. 7D), the assemblage of the former may be reworked (R assemblage; Fig. 18 and Table 2).

*Interpretation*

The recognized AE assemblage is indicative of shallow water settings (Donnici & Serandrei-Barbero, 2002; Mendes *et al.*, 2004; Naish & Kamp, 1997b). The absence of *Quinqueloculina* spp., together with the overall good preservation of the specimens, suggests a relatively low-energy environment featured by low to moderate wave action, that is a lower and/or a middle shoreface, which is consistent with the results from the facies analysis. The occurrence of the R assemblage in Facies B1, where it is associated with Facies B3, supports an upper shoreface setting characterized by occasional pauses in the longshore transport, which is also inferred from the facies analysis.

### Benthic foraminifera assemblages in Facies B3

*Description*

The benthic foraminifera assemblage of Facies B3 usually consists of highly abraded, reworked specimens (R assemblage; Fig. 18 and Table 2). This assemblage is associated with broken bivalve shells, which are characteristic of this facies. In only a few cases, the assemblage found in Facies B3 corresponds to the AE assemblage (MPW section, 38 m WRS, and TAL section, Fig. 18).

*Interpretation*

The occurrence of the R assemblage fits with the inferred high-energy environment on the upper shoreface. Test abrasion and reworking are features expected in an environment characterized by the continuous action of currents leading to dune avalanching, such as observed in Facies B3. The occasional AE assemblage is inferred to be associated with lower energetic conditions and slightly distal settings, between the middle and upper shoreface.

## HEAVY MINERAL ANALYSIS

### Abundance of heavy minerals

The mineralogical analysis enabled the distribution of heavy minerals in the measured sections to be documented (Fig. 18). The heavy mineral assemblage is mainly constituted by garnets and opaque minerals. Other minerals include rutile, zircon, staurolite and tourmaline. The

**Table 2.** Number of benthic micro-foraminifera specimens for 3 g of sediment recognized in the samples analysed. AE, *Ammonia and Elphidium* assemblage; Q, *Quinqueloculina* assemblage; R, reworked assemblage.

| Sample | CBS 1/1 | CBS 1/2 | CBS 1/3 | CBS 1/4 | CBS 1/5 | CBS 1/5/1 | CBS 1/5A | CBS 1/6 | CBS 1/7 | CBS 2/1 | CBS 2/2 | CBS 2/3 | CBS 2/4 | CBW 1 | CBW 2 | CBW 3 | SMS 4 | SMS 4A | SMS 4B | SMS 5 | SMS 5A | SMS 5B | SMS 6 | SMS 7 | SMS A | SMS B | SMS C |
|---|---|---|---|---|---|---|---|---|---|---|---|---|---|---|---|---|---|---|---|---|---|---|---|---|---|---|---|
| Assemblage | AE | Q | AE | AE | AE | | AE | AE | R | AE | Q | AE | AE | AE | Q | AE | R | R | R | R | R | R | R | AE | AE | R | AE |
| **Specimens/3 g** | | | | | | | | | | | | | | | | | | | | | | | | | | | |
| *Ammonia* spp. | 8 | 1 | 6 | 9 | 5 | Barren | 11 | 5 | Reworked | 2 | 1 | 8 | 7 | 7 | | 9 | Reworked | Reworked | Reworked | Reworked | Reworked | Reworked | Reworked | 8 | 5 | Reworked | 6 |
| *Asterigerinata planorbis* | 5 | | 4 | 6 | 6 | | 9 | 1 | | 5 | 1 | 5 | 2 | 2 | | 4 | | | | | | | | 6 | 4 | | 4 |
| *Buccella frigida* | | | | 1 | 1 | | | 1 | | 1 | | | | 1 | | | | | | | | | | | | | |
| *Cibicides lobatulus* | 4 | | 3 | 5 | 1 | | | 1 | | 4 | | 1 | 2 | 2 | | 3 | | | | | | | | 6 | 2 | | 2 |
| *Cibicides refulgens* | 1 | | | 1 | | | 2 | | | 1 | | 1 | | | | | | | | | | | | 4 | | | 1 |
| *Cibicidoides pseudoungerianus* | | | | | | | | | | 1 | | | | | | | | | | | | | | 2 | | | |
| *Cribroelphidium decipiens* | | | | 1 | 1 | | | | | | | 1 | | | | 1 | | | | | | | | | | | |
| *Elphidium advenum* | 1 | | 3 | 2 | 2 | | 2 | 1 | | 2 | | 2 | 2 | 2 | | 2 | | | | | | | | 2 | 2 | | |
| *Elphidium crispum* | 3 | 1 | 3 | 3 | 2 | | 8 | 4 | | 2 | | 12 | 3 | 3 | 1 | 1 | | | | | | | | 9 | 3 | | 4 |
| *Elphidium macellum* | 3 | | 2 | 2 | 2 | | 3 | 5 | | 3 | | 2 | 1 | 4 | | 1 | | | | | | | | 11 | 5 | | 2 |
| *Florilus boueanum* | 4 | 1 | 6 | 7 | 2 | | | | | 2 | 1 | 7 | 4 | 2 | | 4 | | | | | | | | 6 | 8 | | 3 |
| *Lobatula lobatula* | 2 | | 3 | 2 | 1 | | | | | | | | | 1 | | 2 | | | | | | | | 1 | | | |
| *Melonis affinis* | | | 1 | | | | | 1 | | 1 | | | | 1 | | 1 | | | | | | | | | | | |
| *Nonion fabum* | | | 2 | 2 | 1 | | | 1 | | 1 | | 21 | 3 | 2 | | 3 | | | | | | | | 5 | 3 | | |
| *Planulina ariminensis* | 1 | | | 1 | | | | | | 1 | | 1 | | 1 | | | | | | | | | | 3 | 1 | | |
| *Pullenia bulloides* | | | 2 | | | | | 1 | | 2 | | 1 | 1 | | | | | | | | | | | | | | |
| *Rosalina globularis* | 1 | | | | | | | | | | | | | 1 | | 1 | | | | | | | | | | | |
| *Valvulineria bradyana* | 1 | | 1 | | | | | | | 1 | | | | | | 1 | | | | | | | | | | | |
| *Quinqueloculina laevigata* | | 4 | | | | | | | | | 4 | | | | 3 | | | | | | | | | | | | |
| *Quinqueloculina seminulum* | | 3 | | | | | | | | | 4 | | | | 2 | | | | | | | | | | | | |
| *Quinqueloculina* sp. | | 1 | | | | | | | | | 3 | | | | 2 | | | | | | | | | | | | |
| *Sigmoilopsis* sp. | 1 | 1 | | | | | | | | | | | | | | | | | | | | | | | | | |
| *Textularia agglutinans* | | | | | | | | | | 1 | | | | | | 2 | | | | | | | | | | | |
| *Triloculina* sp. | | | | | | | | | | | 2 | | | | 1 | | | | | | | | | | | | |
| *Bulimina* sp. | | | | 2 | | | 1 | | | | | | | | | | | | | | | | | 1 | | | |
| *Uvigerina* sp. | | | 1 | | | | | | | | | | | | | | | | | | | | | | | | |

**Table 2.** (continued)

| Sample | MPW 1 | MPW 1A | MPW 1B | MPW 2 | MPW 3 | MPW 4 | MPW 5 | MPW 6 | MPW 7 | MPW 8 | MPW 8bis | MPW 9 | MPW 10 | MPW 12 | MPW 12A | MPW 13 | MPW 14 | MPW 15 | SAL 1 | SAL 2 | SAL 3 | SAL 4 | SAL 5 | TAL 1 | TAL 2 | TAL 3 | TAL 4 | TAL 5 | TAL 6 |
|---|---|---|---|---|---|---|---|---|---|---|---|---|---|---|---|---|---|---|---|---|---|---|---|---|---|---|---|---|---|
| Assemblage | AE | AE | AE | R | R | AE | AE | R | AE | AE | R | R | R | R | R | R | R | AE | R | R | AE | AE | AE | AE | AE | AE | R | AE | AE |
| **Specimens/3 g** | | | | | | | | | | | | | | | | | | | | | | | | | | | | | |
| *Ammonia* spp. | 10 | 28 | 13 | Reworked | Reworked | 5 | 6 | Reworked | 4 | 7 | Reworked | Reworked | Reworked | Reworked | Reworked | Reworked | Reworked | 7 | Reworked | Reworked | 22 | 8 | 7 | 5 | 9 | 7 | Reworked | 6 | 4 |
| *Asterigerinata planorbis* | 2 | 4 | 2 | | | 2 | 2 | | 2 | 1 | | | | | | | | | | | 2 | 3 | 1 | 2 | 5 | 1 | | | |
| *Buccella frigida* | | | 2 | | | | | | | | | | | | | | | | | | | | | | | | | | |
| *Cibicides lobatulus* | 4 | 2 | 2 | | | 3 | 2 | | 2 | | | | | | | | | | | | 2 | 6 | 2 | 1 | 1 | 1 | | | |
| *Cibicides refulgens* | 2 | 3 | 4 | | | 1 | 2 | | | | | | | | | | | 2 | | | 1 | 2 | 1 | 2 | 2 | | | | |
| *Cibicidoides pseudoungerianus* | 2 | 3 | 4 | | | | | | 1 | | | | | | | | | | | | | 1 | | | | | | | |
| *Cribroelphidium decipiens* | 2 | | | | | | 1 | | | | | | | | | | | | | | | | | | | | | | |
| *Elphidium advenum* | 2 | | | | | 2 | 2 | | | 2 | | | | | | | | | | | | | | | | | | | |
| *Elphidium crispum* | 3 | 8 | 4 | | | 5 | 3 | | 2 | 3 | | | | | | | | 19 | | | 19 | 22 | 16 | 3 | 9 | 15 | | 11 | 13 |
| *Elphidium macellum* | 3 | 5 | 3 | | | 4 | 2 | | 1 | 2 | | | | | | | | 3 | | | 12 | 17 | 8 | 5 | 11 | 7 | | 5 | 7 |
| *Florilus boueanum* | | | 2 | | | 1 | 3 | | 3 | 2 | | | | | | | | 1 | | | | 2 | 1 | 1 | 2 | | | 1 | |
| *Lobatula lobatula* | | | | | | | 1 | | | | | | | | | | | | | | 1 | 2 | 2 | 1 | | | | | |
| *Melonis affinis* | | | | | | 1 | | | 1 | | | | | | | | | | | | | | | | | | | | |
| *Nonion fabum* | | | | | | | 2 | | 2 | | | | | | | | | | | | | | | | | | | | |
| *Planulina ariminensis* | 1 | 1 | 1 | | | | | | 1 | | | | | | | | | | | | | | | | 1 | | | | |
| *Pullenia bulloides* | 1 | | 1 | | | | | | 1 | | | | | | | | | | | | | | | | | | | | |
| *Rosalina globularis* | | | 1 | | | | 1 | | | | | | | | | | | | | | | | | | | | | | |
| *Valvulineria bradyana* | | | 2 | | | 1 | | | | | | | | | | | | | | | | | | | | | | | |
| *Quinqueloculina laevigata* | | | | | | | | | | | | | | | | | | | | | | | | | | | | | |
| *Quinqueloculina seminulum* | | | | | | | | | | | | | | | | | | | | | | | | | | | | | |
| *Quinqueloculina* sp. | | | | | | | | | | | | | | | | | | | | | | | | | | | | | |
| *Sigmoilopsis* sp. | | | | | | | | | | | | | | | | | | | | | | | | | | | | | |
| *Textularia agglutinans* | | 1 | | | | | | | | | | | | | | | | | | | 1 | | | | | | | | |
| *Triloculina* sp. | | | | | | | | | | | | | | | | | | | | | | | | | | | | | |
| *Bulimina* sp. | | | | | | | | | | | | | | | | | | | | | | | | | | | | | |
| *Uvigerina* sp. | | | | | | | | | | | | | | | | | | | | | | | | | | | | | |

abundance of heavy minerals varies significantly, ranging between 173 and 1322 grains per 5 g of sediment (Fig. 18); however, comparing these data with the facies indicates that the distribution of heavy mineral abundance is not random in most cases.

Within any selected section detail, the abundance of heavy minerals is observed to increase within the intervals interpreted as OSBs and occasionally as BSBs, which are both part of Facies A2 (Fig. 18). This increase is minimal in the Casabona (CBS 1, CBS 2 and CBW) sections, and large (up to an order of magnitude) in the MPW section (Fig. 18). In most cases, the increase in heavy minerals is observed just above the WRSs bounding the base of Facies A2 (Fig. 18). A higher abundance of heavy minerals is commonly found in the OSBs characterized by the R foraminifera assemblage, whereas a lower abundance is usually found in the OSBs characterized by the Q assemblage (Fig. 18).

The number of grains of heavy minerals is usually lower than 400 in Facies A1 and in Facies B1 to B3, although a higher abundance, up to *ca* 600 grains, is occasionally found (Fig. 18). A large variability in abundance of heavy minerals is found in Facies A2, outside the intervals interpreted as condensed shell beds (Fig. 18). Significant variations in the abundance of heavy minerals across bedset boundaries, locally found within deposits of facies association B, are not observed (Fig. 18). In the same way, significant variations in abundance of heavy minerals, with respect to the underlying and overlying deposits, have not been recognized within individual storm-related shell beds, such as those found in Facies B1 (samples CBS 1/5A and CBS 2/3; Figs 8A, 8B and 18).

### Mineralogical variations within the sections

The CBS 1 samples are characterized by the presence of garnet and opaques, rare zircon and rutile have been also found. The crystal size is lower than 100 $\mu$m (very fine-grained sand), except in samples CBS 1/6 and CBS 1/7 where they increase their size (medium-grained sand).

The CBS 2 samples are similar to those of the CBS 1 section, but in this case the size of the grains is always very fine-grained sand.

The CBW samples are characterized by the same assemblage with a minor amount of garnet. In sample CBW 2 oxidized material is present. The granulometry is similar to that of the previous cores.

The SAL samples show the same mineralogical assemblage. The amount of garnet, as well as the size of the grains (very fine to medium-grained sand), increases between samples SAL 2 and SAL 3, i.e. in correspondence with the inferred OSB.

In the TAL samples, the mineralogical assemblage is similar to the other samples, and it is characterized by a very fine-grained sand fraction that increases towards the top of the section.

In the MPW section, the usual assemblage is present. Rutile, zircon, staurolite and tourmaline also occur. However, in these samples, garnets occur in two different colours; in the samples below the WRSs, there is the coexistence of orange and pink garnets, while above the WRSs, they are mostly pink. To the top of the section, in samples MPW 13 and MPW 14, oxidized material is present.

The SMS samples are characterized by the same mineralogical assemblage.

## DISCUSSION

### Relationships between bounding surfaces, condensed shell beds, micro-foraminifera assemblages and heavy mineral concentrations

Wave-ravinement surfaces (WRSs) bounding the studied high-frequency sequences (Figs 7 to 10 and 13 to 15) are usually overlain by onlap shell beds (OSBs; part or the whole Facies A2) that document an increase in wave reworking and sediment bypass with respect to the underlying deposits of facies association B (e.g. Kidwell, 1991; Kondo *et al.*, 1998; Naish & Kamp, 1997a), and this is also reflected by an increase in the abundance of heavy minerals and commonly by a change of the micro-foraminifera assemblage (Fig. 18).

The highest abundances of heavy minerals, typically found in the MPW section, are associated with OSBs characterized by large and robust shells (Fig. 13), and with the R foraminifera assemblage (Fig. 18); this evidence points to relatively high-energy as well as significant stratigraphic condensation favoured by low net sedimentation rates, promoting an enrichment of heavy minerals and the reworking of microfauna from older deposits. Moreover, in the MPW section, WRSs mark changes in the mineralogical association, as documented by the shift from both orange and pink garnets (below the

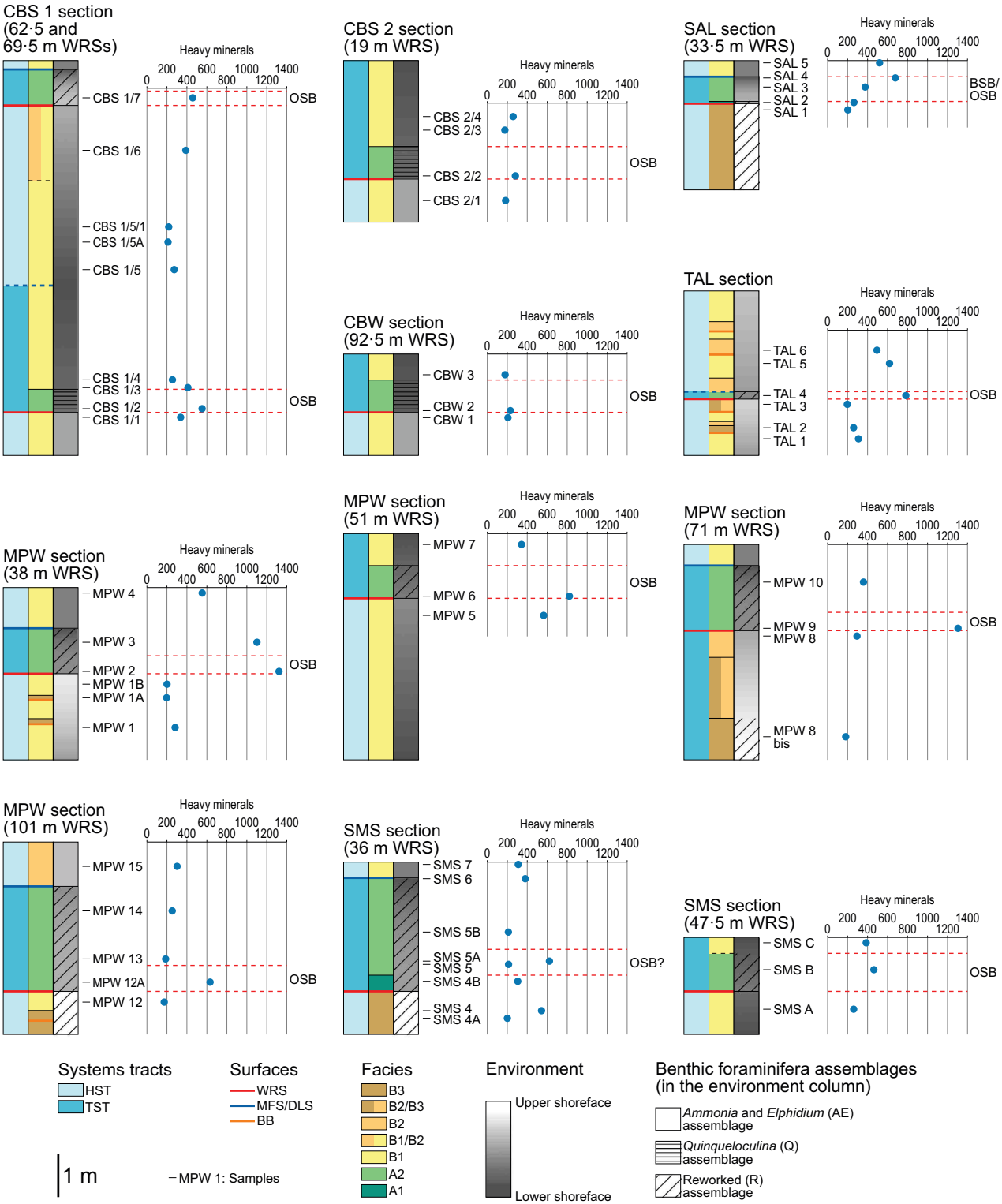


**Fig. 18.** Facies, inferred depositional environments, sequence stratigraphic interpretation, benthic foraminifera assemblages and diagrams with the abundance of heavy minerals (grains per 5 g of sediment). The sediment is richer in heavy minerals within the condensed shell beds that overlie the WRSs (see text). BB, bedset boundary; BSB, backlap shell bed; DLS, downlap surface; HST, highstand systems tract; MFS, maximum flooding surface; OSB, onlap shell bed; TST, transgressive systems tract; WRS, wave-ravinement surface.

WRSs) to mostly pink garnets. In contrast, OSBs associated with average lower values in abundance of heavy minerals, such as those found in the CSB 1, CBS 2 and CBW sections (Fig. 18), are characterized by smaller shells and by the Q assemblage, which point to lower energy levels and probably slightly deeper settings compared to the MPW section. In some cases, inferred condensed shell beds show a variability in abundance of heavy minerals (Fig. 18), and this might reflect local and temporal variations in hydrodynamics and sediment accumulation rate. In one case, the abundance of heavy minerals increases towards the upper part of Facies A2 (SAL section; Figs 9A and 18); this is tentatively interpreted as the consequence of condensation in the context of backlap, leading to the development of a BSB (Kidwell, 1991).

The evidence that individual storm-related shell beds, found in Facies B1, show no variations in both micro-foraminifera assemblages and heavy mineral abundance (see samples CBS 1/5A and CBS 2/3; Figs 8A, 8B and 18) enables the alternative hypothesis that high abundances of heavy minerals are just the result of increased energy during storm events to be ruled out. Prolonged environmental conditions dominated by wave reworking and low net sedimentation rates due to sediment bypass are therefore assumed to be necessary to produce a significant enrichment of heavy minerals in the sediment, and this is a key difference between condensed shell beds, which document several high-energy events, and simple storm beds.

In general, lower increases in the abundance of heavy minerals across WRSs are usually associated with modest environmental changes across those surfaces (Fig. 18). This effect may be related to a combination of factors, including: (i) modest relative sea-level and/or sediment supply changes and associated minor shoreline shifts; (ii) a relatively distal position of the considered section in a downdip transect, preventing a marked facies change in the lower shoreface; and (iii) accumulation in relatively sheltered areas. Minor transgressions are in fact expected to be associated with a lower degree of stratigraphic condensation, and therefore, a lower enrichment of heavy minerals in the OSBs is also expected. Relatively distal positions in a downdip transect are associated with lower wave energy and less sediment bypass during transgression, leading to a lower enrichment of heavy minerals in the transgressive deposits. Sheltered areas also experience lower wave action, promoting a better preservation of lower energy deposits (Zecchin, 2007). In general, these deposits are expected to contain less heavy minerals than those accumulated in less protected (higher energy) areas, due to lower wave erosion (Komar, 2007).

The recognized transgressive lags (Facies A1) do not document a significant increase in abundance of heavy minerals with respect to the underlying and overlying deposits (see the SAL and SMS sections in Fig. 18). It is thought that a relatively rapid burial of these lags by Facies A2 may have prevented a significant enrichment of heavy minerals in the former. In contrast, shell beds composing Facies A2 would represent a longer period of time during the transgressive phase and are genuine condensed deposits.

In contrast to observations across the mapped WRSs, significant differences in micro-foraminifera assemblages and abundance of heavy minerals are not seen above and below bedset boundaries (Fig. 18). This evidence suggests that local variations of energy and/or sediment supply associated with the formation of bedset boundaries are not enough to produce significant environmental changes leading to noticeable variations in micro-foraminifera communities and heavy mineral concentration. Although not recognized in this study, very thin heavy mineral lags may be found at bedset boundaries, and they may be marked by high gamma-ray 'spikes' (Hampson *et al.*, 2008). However, in contrast to the evidence provided by the OSBs, the concentration of heavy minerals in the sediments that overlie the bedset boundaries is in general low.

The comparison between the measured sections highlights that, in general, marked and predictable changes in abundance of heavy minerals from proximal to distal deposits composing facies association B are not found (Fig. 18). Only the CBS 1 section documents a small increase in both heavy mineral abundance and grain size from lower to transitional lower/middle shoreface deposits in facies association B (Fig. 18), as would be expected in a high-energy siliciclastic shoreface-shelf system (Komar, 2007; Komar & Wang, 1984; Kudrass, 1987). The highest concentration of heavy minerals is in fact usually observed in beach sands (Komar, 2007; Roy, 1999), although heavy mineral lags have been recognized in both upper and lower shoreface deposits and are interpreted as the result of minor transgressive episodes and/or reduced sediment supply (Hampson *et al.*, 2008).

In contrast, the abundance of heavy minerals in the upper shoreface deposits (Facies B3) of the studied succession is not much different than that observed in Facies B1 and B2, and in general it is lower than that recognized in the OSBs (Fig. 18). This implies that, although transgressive episodes are inferred to be accompanied by a shift of heavy minerals from the shelf to the beach (Jones & Davies, 1979; Komar, 2007; Roy, 1999), wave reworking and sediment bypass during transgression still enriches the OSBs of heavy minerals with respect to the underlying and overlying regressive deposits.

### Criteria to discriminate between wave-ravinement surfaces and bedset boundaries

Based on geomorphic–stratigraphic criteria, as well as numerical modelling, previous data by Hampson (2000), Storms & Hampson (2005), Hampson *et al.* (2008) and Sømme *et al.* (2008) have suggested that the intra-parasequence (high-frequency sequence) stratigraphy is characterized by bedsets bounded by erosional or non-depositional surfaces that may be the result of changes in wave-climate and sediment supply as well as of minor relative sea-level changes. Moreover, the formation of bedset boundaries is related to a reorganization of the shoreline morphology (Hampson *et al.*, 2008; Sømme *et al.*, 2008). Following this approach, the recognition of sequences and bedsets is therefore mostly based on the scale of observation, lateral continuity and the extent of facies change across bounding surfaces, rather than on the occurrence or absence of shoreline shifts (cf. Catuneanu & Zecchin, 2013; Zecchin & Catuneanu, 2013). Bedset boundaries would be associated with little or no facies change (for example, a juxtaposition of adjacent facies), irrespective of the inferred control (autocyclic or allocyclic), whereas sequences would be associated with a large facies change (for example, from upper shoreface to inner shelf deposits) and would exhibit a larger lateral extent. Such a pragmatic approach may be easily applied in the field, although it is arbitrary in terms of the extent of facies change that is necessary to identify a high-frequency sequence versus a bedset (Fig. 1A and B). It is also important to note that the thickness of cycles is not necessarily proportional to their lateral extent, because relatively thin sequences (*ca* 10 m scale) can develop over distances of tens or even hundreds of kilometres across sedimentary basins that host large interior seaways (e.g. Catuneanu *et al.*, 1999, and references therein). Therefore, the thickness of sedimentary cycles (for example, $10^0$ m versus $10^1$ m) cannot be used alone as a criterion to separate bedsets from sequences, or to infer the lateral development of these units solely from the observation of vertical sections.

The approach proposed by Zecchin & Catuneanu (2013) and Catuneanu & Zecchin (2013) to discriminate between bedsets and high-frequency sequences is based on the recognition of shoreline shifts from field/core data; metre-scale sedimentological cycles that form independently of shoreline shifts should be ascribed to bedsets, whereas sequences are associated with shoreline shifts and are composed of systems tracts. Since the formation of bedset boundaries is typically associated with local autocyclic factors that do not lead to shoreline shifts, their extent along both depositional dip and strike is expected to be limited, as observed by Hampson *et al.* (2008).

The ability to recognize shoreline shifts and the associated transgressive and/or regressive trends therefore represents the critical factor to discriminate between high-frequency sequences and bedsets (Catuneanu & Zecchin, 2013; Zecchin & Catuneanu, 2013). Data from the Belvedere Formation provide key evidence to establish criteria to recognize shoreline shifts in shallow-marine deposits showing limited facies changes across boundaries. In particular, the integration of the available sedimentological, micropalaeontological and mineralogical data provides a powerful tool to investigate at the intra high-frequency sequence scale (Fig. 18). Such an approach affords the acquisition of key data that allow to discriminate between high-frequency WRSs and erosional bedset boundaries, and therefore between high-frequency sequences and bedsets.

From a purely sedimentological and stratigraphic standpoint, several features allow discrimination between high-frequency sequences and bedsets (Fig. 19), even where shoreline shifts cannot be directly observed in the field. In particular, bedsets are composed of deposits accumulated only in one depositional environment, in the upper, middle or lower shoreface, or at the transition between them (Figs 7A, 7D, 9B and 18), whereas sequences document greater environmental changes, especially across sequence boundaries (Figs 7 to 10 and 18). In

| | | High-frequency sequences | Bedsets |
|---|---|---|---|
| *Environmental changes across bounding surfaces* | | Larger | Modest |
| *Water depth changes* | | Present | Absent |
| *Condensed deposits* | | Present | Absent |
| *Physical appearance of the bounding surfaces* | | Good | Modest |
| *Substrate-controlled ichnofacies at bounding surfaces* | | Well developed | Modest |
| *Thickness* | | m- to dam-scale | dm- to m-scale |
| *Changes across bounding surfaces* | *Micro-foraminifera assemblages* | Observed | No changes |
| | *Heavy minerals* | Increase | No changes |

**Fig. 19.** Summary of the sedimentological/stratigraphic, micropalaeontological and mineralogical criteria to discriminate between high-frequency sequences and bedsets, based on data from the Belvedere Formation (see text).

some cases, sequences may also exhibit modest environmental shifts, if they are controlled by minor relative sea-level and/or sediment supply changes, and can often be characterized by condensed deposits in their transgressive interval, whereas bedsets are not (Figs 7 to 10 and 18). Bedset boundaries are not associated with water-depth changes but with only local variations of wave and/or current regime (i.e. environmental energy; Figs 7A, 7D, 9B and 18), as highlighted by Zecchin & Catuneanu (2013) and Catuneanu & Zecchin (2013). In general, bedset boundaries are much less prominent than the WRSs separating facies associations A and B, and the thickness of the bedsets is an order of magnitude lower than that of the high-frequency sequences (Figs 7A, 7D, 9B, 17 and 18). Moreover, substrate-controlled ichnofacies are much more developed where associated with WRSs (Figs 7A, 7C, 8, 9B, 13 and 14).

The sedimentological/stratigraphic evidence is significantly reinforced if combined with the micropalaeontological and mineralogical evidence. In particular, micro-foraminifera assemblages tend to change across WRSs, documenting a shift to more energetic conditions, whereas this evidence is usually absent across bedset boundaries (Fig. 18). Moreover, this change of micro-foraminifera assemblage across WRSs is not observed if both the underlying and overlying deposits contain mostly reworked specimens, documenting overall high-energy environmental conditions (Fig. 18).

The most striking feature, when combined with sedimentological and micropalaeontological data, is the content of heavy minerals in the sediment which represents a key parameter to discriminate between high-frequency sequences and bedsets. As documented in the present case study, the abundance of heavy minerals usually increases across WRSs (Fig. 18), while this increase does not occur across bedset boundaries. The different criteria to discriminate between high-frequency sequences and bedsets are summarized in Fig. 19.

The recognition of erosional surfaces marked by well-developed substrate-controlled ichnofacies and overlain by condensed shell beds, and which document changes of environment/depth and micro-foraminifera assemblages, as well as an increase in heavy minerals across them, represents the best evidence to interpret WRSs bounding high-frequency sequences composed of shallow-marine deposits. Furthermore, the integrated approach illustrated here is also expected to help significantly where environmental/water-depth changes across bounding surfaces are more difficult to recognize (Fig. 18), and where substrate-controlled ichnofacies and OSBs are absent or poorly developed.

The results presented in this study show that the criterion recommended by Zecchin & Catuneanu (2013) and Catuneanu & Zecchin (2013) to discriminate between bedsets and high-frequency sequences can be applied in field studies, particularly if an integrated sedimentological, micropalaeontological and mineralogical approach is adopted (Figs 18 and 19). Such an approach significantly increases the ability to discriminate between high-frequency WRSs, or transgressive surfaces in general, and bedset boundaries unrelated to shoreline shifts. Further studies of shallow-marine successions of different ages, and with a cyclicity that exhibits different architectures and thicknesses, would benefit from this integrated approach and may help define additional criteria to recognize shoreline shifts and to understand the controls on the cyclicity.

## Hypothesis on the origin of the cyclicity

Zecchin (2005) suggested that the cyclicity characterizing the Belvedere Formation is related to the Milankovitch precession cycle (*ca* 22 kyr duration), which is well expressed in the lower Pliocene successions of the Mediterranean

(Hilgen & Langereis, 1989). Unfortunately, because the timing of deposition of the Belvedere Formation is poorly constrained, the correlation between the recognized cyclicity and the lower Pliocene precession-driven cyclicity cannot be confirmed definitively. However, the architecture of the fully-shoreface high-frequency sequences composing the Belvedere Formation fits well with the characteristics of the Zanclean precession-driven cyclicity, which mainly affected the climate, leading to alternating dry and wet phases that in turn influenced the sediment supply to the marine realm (Hilgen & Langereis, 1989; Roveri & Taviani, 2003).

Following this hypothesis, the studied high-frequency sequences would primarily be the result of climate-driven sediment supply changes (Figs 7 to 10). The transgressive episodes would have been related to the drier phases, which would have favoured a decrease in the terrigenous input and an increase in the volume of bivalve communities in the deposits of Facies A2 (e.g. Schwarz *et al.*, 2016), so that the transgressive deposits that are not part of the OSBs are still shell-rich (Figs 7A, 7C, 7D, 8A and 10A). In contrast, the wetter phases would have caused an increase in terrigenous input and the accumulation of the HST of the high-frequency sequences. Relatively less dry phases may have favoured the accumulation of transgressive systems tracts (TSTs) composed in part of mostly siliciclastic deposits (Facies B1), as observed in the Casabona motif (Fig. 16A). Eustatic sea-level falls associated with the inferred climate changes would have been counteracted by active fault-controlled subsidence, preventing relative sea-level lowering and the accumulation of the FSST; this may explain the systematic absence of forced regressive deposits within the sequences. More significant relative sea-level changes, combined with tectonic confinement, were probably associated with the migration of the large subaqueous dunes found locally in the Belvedere Formation (i.e. the Type 2 cycles of Zecchin, 2005) (Fig. 5).

## CONCLUSIONS

The integration of sedimentological, micropalaeontological and mineralogical data provides a powerful tool in high-resolution sequence stratigraphic analysis. The application of this approach to the shallow-marine deposits of the lower Pliocene Belvedere Formation, southern Italy, allows a distinction between bedsets, bounded by surfaces that are unrelated to shoreline shifts, and high-frequency sequences bounded by wave-ravinement surfaces. Key criteria to discriminate between wave-ravinement surfaces (WRSs) and bedset boundaries are defined (Fig. 19), and may be grouped into sedimentological/stratigraphic, micropalaeontological and mineralogical criteria.

The sedimentological/stratigraphic criteria include: (i) recognition of environmental changes across bounding surfaces (larger across WRSs, and only associated with short-term energy variations in the case of bedset boundaries); (ii) recognition of water-depth changes across bounding surfaces (absent across bedset boundaries); (iii) occurrence of condensed deposits (absent above bedset boundaries); (iv) physical appearance (more prominent in the case of WRSs and associated substrate-controlled ichnofacies); (v) cycle thickness (an order of magnitude greater for the high-frequency sequences). An additional, previously documented criterion, is the limited lateral extent of bedset boundaries relative to WRSs and transgressive surfaces.

These qualitative criteria may be combined with the micropalaeontological and mineralogical evidence to achieve a more reliable discrimination between WRSs and bedset boundaries. In particular, micro-foraminifera assemblages may change across WRSs, documenting a shift to more energetic conditions, whereas this evidence is absent across bedset boundaries. Moreover, the abundance of heavy minerals usually increases across WRSs, reaching a maximum within condensed deposits, whereas this increase does not occur across bedset boundaries. Wave reworking and low net sedimentation rates due to sediment bypass during transgression are thought to be the processes that lead to an enrichment of heavy minerals in the condensed transgressive deposits.

It is stressed that both the micropalaeontological and mineralogical evidence, if considered individually, cannot be used as sole indicators to discriminate between WRSs and bedset boundaries; it is their integration with the sedimentological/stratigraphic evidence that affords reliable results. The illustrated integrated approach may be used in all high-resolution sequence stratigraphic studies based on outcrop and/or core data, allowing one to better understand the architecture and hierarchical framework of small-scale cycles, as well as to predict

the distribution and extent of porous shallow-marine sedimentary bodies.

## ACKNOWLEDGEMENTS

We thank Oliver Jordan, Domenico Chiarella and Peter Flaig, and the Editors Nigel Mountney and Piret Plink-Björklund, for helpful and constructive comments during the review process.

## REFERENCES

**Abbott, S.T.** (1997) Mid-cycle condensed shellbeds from mid-Pleistocene cyclothems, New Zealand: implications for sequence architecture. *Sedimentology*, **44**, 805–824.

**Abbott, S.T.** and **Carter, R.M.** (1994) The sequence architecture of mid-Pleistocene (c.1.1.-0.4 Ma) cyclothems from New Zealand: facies development during a period of orbital control on sea-level cyclicity. In: *Orbital Forcing and Cyclic Sequences* (Eds P.L. De Boer and D.G. Smith), *IAS Spec. Publ.*, **19**, 367–394.

**Amodio Morelli, L.**, **Bonardi, G.**, **Colonna, V.**, **Dietrich, D.**, **Giunta, G.**, **Ippolito, F.**, **Liguori, V.**, **Lorenzoni, S.**, **Paglionico, A.**, **Perrone, V.**, **Picarretta, G.**, **Russo, M.**, **Scandone, P.**, **Zanettin-Lorenzoni, E.** and **Zuppetta, A.** (1976) L'Arco Calabro-Peloritano nell'orogene Appenninico-Maghrebide. *Mem. Soc. Geol. It.*, **17**, 1–60.

**Bonardi, G.**, **Cavazza, W.**, **Perrone, V.** and **Rossi, S.** (2001) Calabria-Peloritani terrane and northern Ionian Sea. In: *Anatomy of an Orogen: The Apennines and Adjacent Mediterranean Basins* (Eds G.B. Vai and I.P. Martini), pp. 287–306. Kluwer Academic Publishers, Bodmin.

**Cantalamessa, G.**, **Di Celma, C.** and **Ragaini, L.** (2005) Sequence stratigraphy of the Punta Ballena Member of the Jama Formation (Early Pleistocene, Ecuador): insights from integrated sedimentologic, taphonomic and paleoecologic analysis of molluscan shell concentrations. *Palaeogeogr. Palaeoclimatol. Palaeoecol.*, **216**, 1–25.

**Cattaneo, A.** and **Steel, R.J.** (2003) Transgressive deposits: a review of their variability. *Earth-Sci. Rev.*, **62**, 187–228.

**Catuneanu, O.** (2003) *Sequence Stratigraphy of Clastic Systems*. Geological Association of Canada, Short Course Notes Volume **16**, 248 pp.

**Catuneanu, O.** (2006) *Principles of Sequence Stratigraphy*. Elsevier, Amsterdam. 386 pp.

**Catuneanu, O.** and **Biddulph, M.N.** (2001) Sequence stratigraphy of the Vaal Reef facies associations in the Witwatersrand foredeep, South Africa. *Sed. Geol.*, **141–142**, 113–130.

**Catuneanu, O.** and **Zecchin, M.** (2013) High-resolution sequence stratigraphy of clastic shelves II: controls on sequence development. *Mar. Pet. Geol.*, **39**, 26–38.

**Catuneanu, O.**, **Sweet, A.R.** and **Miall, A.D.** (1999) Concept and styles of reciprocal stratigraphies: Western Canada foreland basin. *Terra Nova*, **11**, 1–8.

**Catuneanu, O.**, **Abreu, V.**, **Bhattacharya, J.P.**, **Blum, M.D.**, **Dalrymple, R.W.**, **Eriksson, P.G.**, **Fielding, C.R.**, **Fisher, W.L.**, **Galloway, W.E.**, **Gibling, M.R.**, **Giles, K.A.**, **Holbrook, J.M.**, **Jordan, R.**, **Kendall, C.G.**, **St, C.**, **Macurda, B.**, **Martinsen, O.J.**, **Miall, A.D.**, **Neal, J.E.**, **Nummedal, D.**, **Pomar, L.**, **Posamentier, H.W.**, **Pratt, B.R.**, **Sarg, J.F.**, **Shanley, K.W.**, **Steel, R.J.**, **Strasser, A.**, **Tucker, M.E.** and **Winker, C.** (2009) Towards the standardization of sequence stratigraphy. *Earth-Sci. Rev.*, **92**, 1–33.

**Cavazza, W.** and **Barone, M.** (2010) Large-scale sedimentary recycling of tectonic mélange in a forearc setting: the Ionian basin (Oligocene-Quaternary, southern Italy). *Geol. Soc. Am. Bull.*, **122**, 1932–1949.

**Cavazza, W.** and **DeCelles, P.G.** (1993) Miocene submarine canyons and associated sedimentary facies in south-eastern Calabria, southern Italy. *Geol. Soc. Am. Bull.*, **105**, 1297–1309.

**Chiarella, D.** and **Longhitano, S.G.** (2012) Distinguishing depositional environments in shallow-water mixed, bio-siliciclastic deposits on the basis of the degree of heterolithic segregation (Gelasian, southern Italy). *J. Sed. Res.*, **82**, 969–990.

**Cita, M.B.** (1975) Studi sul Pliocene e sugli strati di passaggio dal Miocene al Pliocene. VIII. Planktonic foraminiferal biozonation of the Mediterranean Pliocene deep-sea record. A revision. *Riv. Ital. Paleontol. Stratigr.*, **81**, 527–544.

**Clifton, H.E.** (1981) Progradational sequences in Miocene shoreline deposits, southeastern Caliente Range, California. *J. Sed. Petrol.*, **51**, 165–184.

**Clifton, H.E.** (2006) A reexamination of facies models for clastic shorelines. In: *Facies Models Revisited* (Eds H.W. Posamentier and R.G. Walker), *SEPM Spec. Publ.*, **84**, 293–337.

**Consolaro, C.**, **Macrì, P.**, **Massari, F.**, **Speranza, F.** and **Fornaciari, E.** (2013) A major change in the sedimentation regime in the Crotone Basin (Southern Italy) around 3.7-3.6 Ma. *Palaeogeogr. Palaeoclimatol. Palaeoecol.*, **392**, 398–410.

**Cosentino, D.**, **Gliozzi, E.** and **Salvini, F.** (1989) Brittle deformations in the Upper Pleistocene deposits of the Crotone Peninsula, Calabria, southern Italy. *Tectonophysics*, **163**, 205–217.

**Datta, B.**, **Sarkar, S.** and **Chaudhuri, A.K.** (1999) Swaley cross-stratification in medium to coarse sandstone produced by oscillatory and combined flows: examples from the Proterozoic Kansapathar Formation, Chhattisgarh Basin, M.P., India. *Sed. Geol.*, **129**, 51–70.

**Demarest, J.M.** and **Kraft, J.C.** (1987) Stratigraphic record of Quaternary sea levels: implications for more ancient strata. In: *Sea-Level Fluctuation and Coastal Evolution* (Eds D. Nummedal, O.H. Pilkey and J.D. Howard), *SEPM Spec. Publ.*, **41**, 223–239.

**Di Celma, C.** and **Cantalamessa, G.** (2007) Sedimentology and high-frequency sequence stratigraphy of a forearc extensional basin: the Miocene Caleta Herradura Formation, Mejillones Peninsula, northern Chile. *Sed. Geol.*, **198**, 29–52.

**Di Celma, C.**, **Ragaini, L.**, **Cantalamessa, G.** and **Landini, W.** (2005) Basin physiography and tectonic influence on the sequence architecture and stacking pattern: Pleistocene succession of the Canoa Basin (central Ecuador). *Geol. Soc. Am. Bull.*, **117**, 1226–1241.

**Donnici, S.** and **Serandrei-Barbero, R.** (2002) The benthic foraminiferal communities of the North Adriatic continental shelf. *Mar. Micropaleontol.*, **44**, 93–123.

**Dott, R.H.** and **Bourgeois, J.** (1982) Hummocky stratification: significance of its variable bedding sequences. *Geol. Soc. Am. Bull.*, **93**, 663–680.

**Dumas, S.** and **Arnott, R.W.C.** (2006) Origin of hummocky and swaley cross-stratification – The controlling influence of unidirectional current strength and aggradation rate. *Geology*, **34**, 1073–1076.

**Dumas, S.**, **Arnott, R.W.C.** and **Southard, J.B.** (2005) Experiments on oscillatory-flow and combined-flow bed forms: implications for interpreting parts of the shallow-marine sedimentary record. *J. Sed. Res.*, **75**, 501–513.

**Faccenna, C.**, **Becker, T.W.**, **Lucente, F.P.**, **Jolivet, L.** and **Rossetti, F.** (2001) History of subduction and back-arc extension in the Central Mediterranean. *Geophys. J. Int.*, **145**, 809–820.

**Faccenna, C.**, **Piromallo, C.**, **Crespo-Blanc, A.**, **Jolivet, L.** and **Rossetti, F.** (2004) Lateral slab deformation and the origin of the western Mediterranean arcs. *Tectonics*, **23**, TC1012. https://doi.org/10.1029/C001488.

**Fürsich, F.T.** and **Pandey, D.K.** (1999) Genesis and environmental significance of Upper Cretaceous shell concentrations from the Cauvery Basin, southern India. *Palaeogeogr. Palaeoclimatol. Palaeoecol.*, **145**, 119–139.

**Gibbard, P.L.**, **Head, M.J.**, **Walker, M.J.C.** and The Subcommission on Quaternary Stratigraphy (2010) Formal ratification of the Quaternary System/Period and the Pleistocene Series/Epoch with a base at 2.58 Ma. *J. Quat. Sci.*, **25**, 96–102.

**Hampson, G.J.** (2000) Discontinuity surfaces, clinoforms, and facies architecture in a wave-dominated, shoreface-shelf parasequence. *J. Sed. Res.*, **70**, 325–340.

**Hampson, G.J.** and **Storms, J.E.A.** (2003) Geomorphological and sequence stratigraphic variability in wave-dominated, shoreface-shelf parasequences. *Sedimentology*, **50**, 667–701.

**Hampson, G.J.**, **Rodriguez, A.B.**, **Storms, J.E.A.**, **Johnson, H.D.** and **Meyer, C.T.** (2008) Geomorphology and high-resolution stratigraphy of progradational wave-dominated shoreline deposits: impact on reservoir-scale facies architecture. In: *Recent Advances in Models of Siliciclastic Shallow-Marine Stratigraphy* (Eds G.J. Hampson, R.J. Steel, P.M. Burgess and R.W. Dalrymple), *SEPM Spec. Publ.*, **90**, 117–142.

**Hampson, G.J.**, **Gani, M.R.**, **Sharman, K.E.**, **Irfan, N.** and **Bracken, B.** (2011) Along-strike and down-dip variations in shallow-marine sequence stratigraphic architecture: Upper Cretaceous Star Point Sandstone, Wasatch Plateau, central Utah, U.S.A. *J. Sed. Res.*, **81**, 159–184.

**Hart, B.S.** and **Plint, A.G.** (1995) Gravelly shoreface and beachface deposits. In: *Sedimentary Facies Analysis* (Ed. A.G. Plint), *IAS Spec. Publ.*, **22**, 75–99.

**Hilgen, F.J.** and **Langereis, C.G.** (1989) Periodicities of $CaCO_3$ cycles in the Pliocene of Sicily: discrepancies with the quasi-periods of the Earth's orbital cycles? *Terra Nova*, **1**, 409–415.

**Hwang, I.-G.** and **Heller, P.L.** (2002) Anatomy of a transgressive lag: Panther Tongue Sandstone, Star Point Formation, central Utah. *Sedimentology*, **49**, 977–999.

**Johnson, H.D.** and **Baldwin, C.T.** (1996) Shallow clastic seas. In: *Sedimentary Environments: Processes, Facies and Stratigraphy* (Ed. H.G. Reading), pp. 232–280. Blackwell Science, Oxford.

**Jones, H.A.** and **Davies, P.J.** (1979) Preliminary studies of offshore placer deposits, eastern Australia. *Mar. Geol.*, **30**, 243–268.

**Kidwell, S.M.** (1991) Condensed deposits in siliciclastic sequences: expected and observed features. In: *Cycles and Events in Stratigraphy* (Eds G. Einsele, W. Ricken and A. Seilacher), pp. 682–695. Springer-Verlag, Berlin.

**Knott, S.D.** and **Turco, E.** (1991) Late Cenozoic kinematics of the Calabrian Arc, southern Italy. *Tectonics*, **10**, 1164–1172.

**Komar, P.D.** (2007) The entrainment, transport and sorting of heavy minerals by waves and currents. In: *Heavy Minerals in Use* (Eds M.A. Mange and D.T. Wright), *Development in Sedimentology*, **58**, 3–48.

**Komar, P.D.** and **Wang, C.** (1984) Processes of selective grain transport and the formation of placers on beaches. *J. Geol.*, **92**, 637–655.

**Kondo, Y.**, **Abbott, S.T.**, **Kitamura, A.**, **Kamp, P.J.J.**, **Naish, T.R.**, **Kamataki, T.** and **Saul, G.S.** (1998) The relationship between shellbed type and sequence architecture: examples from Japan and New Zealand. *Sed. Geol.*, **122**, 109–127.

**Kudrass, H.R.** (1987) Sedimentary models to estimate the heavy-mineral potential of shelf sediments. In: *Marine Minerals: Advances in Research and Resource Assessment* (Eds P.G. Teleki, M.R. Dobson, J.R. Moore and U. von Stackelberg), *NATO Advanced Study Institutes Series, Series C, Mathematical and Physical Sciences*, pp. 588.

**Leckie, D.A.** and **Walker, R.G.** (1982) Storm- and tide-dominated shorelines in Cretaceous Moosebar-Lower Gates interval-outcrop equivalents of deep basin gas trap in Western Canada. *AAPG Bull.*, **66**, 138–157.

**Leithold, E.L.** and **Bourgeois, J.** (1984) Characteristics of coarse-grained sequences deposited in nearshore, wave-dominated environments – examples from the Miocene of south-west Oregon. *Sedimentology*, **31**, 749–775.

**Loeblich, A.R.** and **Tappan, H.** (1987) *Foraminiferal Genera and Their Classification*. Van Nostrand Reinhold Company, New York. 970 pp.

**Longhitano, S.G.**, **Chiarella, D.** and **Muto, F.** (2014) Three-dimensional to two-dimensional cross-strata transition in the lower Pleistocene Catanzaro tidal strait transgressive succession (southern Italy). *Sedimentology*, **61**, 2136–2171.

**Lourens, L.J.**, **Antonarakou, A.**, **Hilgen, F.J.**, **Van Hoof, A.A.M.**, **Vergnaud-Grazzini, C.** and **Zachariasse, W.J.** (1996) Evaluation of the Plio-Pleistocene astronomical timescale. *Paleoceanography*, **11**, 391–413.

**MacEachern, J.A.** and **Bann, K.L.** (2008) The role of ichnology in refining shallow marine facies models. In: *Recent Advances in Models of Siliciclastic Shallow-Marine Stratigraphy* (Eds G.J. Hampson, R.J. Steel, P.M. Burgess and R.W. Dalrymple), *SEPM Spec. Publ.*, **90**, 73–116.

**Malinverno, A.** and **Ryan, W.B.F.** (1986) Extension in the Tyrrhenian Sea and shortening in the Apennines as a result of arc migration driven by sinking of the lithosphere. *Tectonics*, **5**, 227–245.

**Massari, F.** and **Parea, G.C.** (1988) Progradational gravel beach sequences in a moderate- to high-energy, microtidal marine environment. *Sedimentology*, **35**, 881–913.

**Massari, F.** and **Prosser, G.** (2013) Late Cenozoic tectono-stratigraphic sequences of the Crotone Basin: insights on the geodynamic history of the Calabrian arc and Tyrrhenian Sea. *Basin Res.*, **25**, 26–51.

**Mellere, D.**, **Zecchin, M.** and **Perale, C.** (2005) Stratigraphy and sedimentology of fault-controlled backstepping shorefaces, middle Pliocene of Crotone Basin, Southern Italy. *Sed. Geol.*, **176**, 281–303.

**Mendes, I.**, **Gonzalez, R.**, **Dias, J.M.A.**, **Lobo, F.** and **Martins, V.** (2004) Factors influencing recent benthic foraminifera distribution on the Guadiana shelf (Southwestern Iberia). *Mar. Micropaleontol.*, **51**, 171–192.

**Meulenkamp, J.E.**, **Hilgen, F.** and **Voogt, E.** (1986) Late Cenozoic sedimentary tectonic history of the Calabrian Arc. *Giorn. Geol.*, **48**, 345–359.

**Naish, T.R.** and **Kamp, P.J.J.** (1997a) Sequence stratigraphy of sixth-order (41 k.y.) Pliocene-Pleistocene cyclothems, Wanganui basin, New Zealand: a case for the regressive systems tract. *Geol. Soc. Am. Bull.*, **109**, 978–999.

**Naish, T.** and **Kamp, P.J.J.** (1997b) Foraminiferal depth palaeoecology of Late Pliocene shelf sequences and system tracts, Wanganui Basin, New Zealand. *Sed. Geol.*, **110**, 237–255.

**Norris, R.D.** (1986) Taphonomic gradients in shelf fossil assemblages: pliocene Purisima Formation, California. *Palaios*, **1**, 256–270.

**Nummedal, D.** and **Swift, D.J.P.** (1987) Transgressive stratigraphy at sequence-bounding unconformities: some principles derived from Holocene and Cretaceous examples. In: *Sea-Level Fluctuation and Coastal Evolution* (Eds D. Nummedal, O.H. Pilkey and J.D. Howard), *SEPM Spec. Publ.*, **41**, 241–260.

**Pemberton, S.G.**, **MacEachern, J.A.** and **Frey, R.W.** (1992) Trace fossil facies models: environmental and allostratigraphic significance. In: *Facies Models: Response to Sea Level Change* (Eds R.G. Walker and N.P. James), pp. 47–72. Geological Association of Canada, Toronto.

**Plint, A.G.** (1988) Sharp-based shoreface sequences and offshore bars in the Cardium Formation of Alberta; their relationship to relative changes in sea level. In: *Sea Level Changes: An Integrated Approach* (Eds C.K. Wilgus, B.S. Hastings, C.G.St.C. Kendall, H.W. Posamentier, C.A. Ross and J.C. Van Wagoner), *SEPM Spec. Publ.*, **42**, 357–370.

**Plint, A.G.** and **Nummedal, D.** (2000) The falling stage systems tract: recognition and importance in sequence stratigraphic analysis. In: *Sedimentary Responses to Forced Regressions* (Eds D. Hunt and R.L. Gawthorpe), *Geol. Soc. Spec. Publ.*, **172**, 1–17.

**Posamentier, H.W.** and **Allen, G.P.** (1999) *Siliciclastic Sequence Stratigraphy – Concepts and Applications*. SEPM Conc. Sedim. Paleont., Tulsa, OK, USA, vol. **7**, 210 pp.

**Raffi, I.**, **Backman, J.**, **Fornaciari, E.**, **Pälike, H.**, **Rio, D.**, **Lourens, L.** and **Hilgen, F.** (2006) A review of calcareous nannofossil astrobiochronology encompassing the past 25 million years. *Quatern. Sci. Rev.*, **25**, 3113–3137.

**Reading, H.G.** and **Collinson, J.D.** (1996) Clastic coasts. In: *Sedimentary Environments: Processes, Facies and Stratigraphy* (Ed. H.G. Reading), pp. 154–231. Blackwell Science, Oxford.

**Rio, D.**, **Raffi, I.** and **Villa, G.** (1990) Pliocene-Pleistocene calcareous nannofossil distribution patterns in the western Mediterranean. In: *Proceedings of the Ocean Drilling Program, Scientific Results* (Eds K.A. Kastens and J. Mascle *et al.*), Vol. **107**, pp. 513–533. Ocean Drilling Program, College Station, TX.

**Roda, C.** (1964) Distribuzione e facies dei sedimenti Neogenici nel Bacino Crotonese. *Geol. Romana*, **3**, 319–366.

**Roveri, M.** and **Taviani, M.** (2003) Calcarenite and sapropel deposition in the Mediterranean Pliocene: shallow- and deep-water record of astronomically driven climatic events. *Terra Nova*, **15**, 279–286.

**Roy, P.S.** (1999) Heavy mineral beach placers in southeastern Australia: their nature and genesis. *Econ. Geol.*, **94**, 567–588.

**Samir, A.M.**, **Abdou, H.F.**, **Zazou, S.M.** and **El-Menhawey, W.H.** (2003) Cluster analysis of recent benthic foraminifera from the northwestern Mediterranean coast of Egypt. *Rev. Micropaléontol.*, **46**, 111–130.

**Sartori, R.** (2003) The Tyrrhenian back-arc basin and subduction of the Ionian lithosphere. *Episodes*, **26**, 217–221.

**Saul, G.**, **Naish, T.R.**, **Abbott, S.T.** and **Carter, R.M.** (1999) Sedimentary cyclicity in the marine Pliocene-Pleistocene of the Wanganui basin (New Zealand): sequence stratigraphic motifs characteristic of the past 2.5 m.y. *Geol. Soc. Am. Bull.*, **111**, 524–537.

**Schwarz, E.**, **Veiga, G.D.**, **Alvarez Trentini, G.** and **Spalletti, L.** (2016) Climatically versus eustatically controlled, sediment-supply-driven cycles: carbonate-siliciclastic, high-frequency sequences in the Valanginian of the Neuquén Basin (Argentina). *J. Sed. Res.*, **86**, 312–335.

**Serandrei-Barbero, R.**, **Albani, A.** and **Bonardi, M.** (2004) Ancient and modern salt marshes in the Lagoon of Venice. *Palaeogeogr. Palaeoclimatol. Palaeoecol.*, **202**, 229–244.

**Sømme, T.O.**, **Howell, J.A.**, **Hampson, G.J.** and **Storms, J.E.A.** (2008) Genesis, architecture, and numerical modeling of intra-parasequence discontinuity surfaces in wave-dominated deltaic deposits: Upper Cretaceous Sunnyside Member, Blackhawk Formation, Book Cliffs, Utah, U.S.A. In: *Recent Advances in Models of Siliciclastic Shallow-Marine Stratigraphy* (Eds G.J. Hampson, R.J. Steel, P.M. Burgess and R.W. Dalrymple), *SEPM Spec. Publ.*, **90**, 421–441.

**Steel, R.J.**, **Rasmussen, H.**, **Eide, S.**, **Neuman, B.** and **Siggerud, E.I.H.** (2000) Anatomy of high-sediment-supply, transgressive tracts in the Vilomara composite sequence, Sant Llorenc del Munt, Ebro basin, NE Spain. *Sed. Geol.*, **138**, 125–142.

**Storms, J.E.A.** and **Hampson, G.J.** (2005) Mechanisms for forming discontinuity surfaces within shoreface–shelf parasequences: sea level, sediment supply, or wave regime? *J. Sed. Res.*, **75**, 67–81.

**Swift, D.J.P.** (1968) Coastal erosion and transgressive stratigraphy. *J. Geol.*, **76**, 444–456.

**Van Dijk, J.P.** (1990) Sequence stratigraphy, kinematics and dynamic geohistory of the Crotone Basin (Calabria Arc, Central Mediterranean): an integrated approach. *Mem. Soc. Geol. It.*, **44**, 259–285.

**Van Dijk, J.P.** (1991) Basin dynamics and sequence stratigraphy in the Calabrian Arc (Central Mediterranean): records and pathways of the Crotone Basin. *Geol. Mijnbouw*, **70**, 187–201.

**Van Dijk, J.P.** (1994) Late Neogene kinematics of intra-arc oblique shear zones: the Petilia-Rizzuto Fault Zone (Calabrian Arc, Central Mediterranean). *Tectonics*, **13**, 1201–1230.

**Van Dijk, J.P.** and **Okkes, F.W.M.** (1991) Neogene tectonostratigraphy and kinematics of Calabrian basins; implications for the geodynamics of the Central Mediterranean. *Tectonophysics*, **196**, 23–60.

**Van Wagoner, J.C.**, **Posamentier, H.W.**, **Mitchum, R.M.**, **Vail, P.R.**, **Sarg, J.F.**, **Loutit, T.S.** and **Hardenbol, J.** (1988) An overview of the fundamentals of sequence stratigraphy and key definitions. In: *Sea Level Changes: An Integrated Approach* (Eds C.K. Wilgus, B.S. Hastings, C.G.St.C. Kendall, H.W. Posamentier, C.A. Ross and J.C. Van Wagoner), *SEPM Spec. Publ.*, **42**, 39–45.

**Van Wagoner, J.C.**, **Mitchum, R.M.**, **Campion, K.M.** and **Rahmanian, V.D.** (1990) *Siliciclastic Sequence Stratigraphy in Well Logs, Cores, and Outcrops*. Tulsa, OK, USA: AAPG Met. Expl., **7**, 55 pp.

**Westaway, R.** (1993) Quaternary uplift of Southern Italy. *J. Geophys. Res.*, **98**, 21741–21772.

**Zecchin, M.** (2005) Relationships between fault-controlled subsidence and preservation of shallow-marine small-scale

cycles: example from the lower Pliocene of the Crotone Basin (southern Italy). *J. Sed. Res.*, **75**, 300–312.

**Zecchin, M.** (2007) The architectural variability of small-scale cycles in shelf and ramp clastic systems: the controlling factors. *Earth-Sci. Rev.*, **84**, 21–55.

**Zecchin, M.** and **Caffau, M.** (2012) The vertical compartmentalization of reservoirs: an example from a outcrop analog, Crotone Basin, southern Italy. *AAPG Bull.*, **96**, 155–175.

**Zecchin, M.** and **Catuneanu, O.** (2013) High-resolution sequence stratigraphy of clastic shelves I: units and bounding surfaces. *Mar. Pet. Geol.*, **39**, 1–25.

**Zecchin, M.** and **Catuneanu, O.** (2015) High-resolution sequence stratigraphy of clastic shelves III: applications to reservoir geology. *Mar. Pet. Geol.*, **62**, 161–175.

**Zecchin, M.**, **Massari, F.**, **Mellere, D.** and **Prosser, G.** (2003) Architectural styles of prograding wedges in a tectonically active setting, Crotone Basin, Southern Italy. *J. Geol. Soc.*, **160**, 863–880.

**Zecchin, M.**, **Massari, F.**, **Mellere, D.** and **Prosser, G.** (2004) Anatomy and evolution of a Mediterranean-type fault bounded basin: the Lower Pliocene of the northern Crotone Basin (Southern Italy). *Basin Res.*, **16**, 117–143.

**Zecchin, M.**, **Mellere, D.** and **Roda, C.** (2006) Sequence stratigraphy and architectural variability in growth fault-bounded basin fills: a review of Plio-Pleistocene stratal units of the Crotone Basin (southern Italy). *J. Geol. Soc.*, **163**, 471–486.

**Zecchin, M.**, **Brancolini, G.**, **Tosi, L.**, **Rizzetto, F.**, **Caffau, M.** and **Baradello, L.** (2009) Anatomy of the Holocene succession of the southern Venice Lagoon revealed by very high resolution seismic data. *Cont. Shelf Res.*, **29**, 1343–1359.

**Zecchin, M.**, **Caffau, M.**, **Civile, D.**, **Critelli, S.**, **Di Stefano, A.**, **Maniscalco, R.**, **Muto, F.**, **Sturiale, G.** and **Roda, C.** (2012) The Plio-Pleistocene evolution of the Crotone Basin (southern Italy): interplay between sedimentation, tectonics and eustasy in the frame of Calabrian Arc migration. *Earth-Sci. Rev.*, **115**, 273–303.

**Zecchin, M.**, **Praeg, D.**, **Ceramicola, S.** and **Muto, F.** (2015) Onshore to offshore correlation of regional unconformities in the Plio-Pleistocene sedimentary successions of the Calabrian Arc (central Mediterranean). *Earth-Sci. Rev.*, **142**, 60–78.

**Zecchin, M.**, **Caffau, M.** and **Ceramicola, S.** (2016) Interplay between regional uplift and glacio-eustasy in the Crotone Basin (Calabria, southern Italy) since 0.45 Ma: a review. *Global Planet. Change*, **143**, 196–213.

*Revision accepted 28 March 2017*